Revision 1

Effect of magnesium on monohydrocalcite formation and unit cell parameters

Oleg S. Vereshchagin[1,*], Olga V. Frank-Kamenetskaya[1], Maria A. Kuz'mina[1],

Irina A. Chernyshova[1], Vladimir V. Shilovskikh[2,3]

[1]Institute of Earth Sciences, St. Petersburg State University, University Emb. 7/9,

199034 St. Petersburg, Russia.

[2]Geomodel Centre, St. Petersburg State University, Uliyanovskaya St. 1,

198504, St. Petersburg, Russia

[3]Institute of Mineralogy, Urals Branch of the Russian Academy of Sciences, Miass 456317,

Russia

*E-mail: o.vereshchagin@spbu.ru

ABSTRACT

Monohydrocalcite (MHC) is hydrated calcium carbonate, which plays an active role in many geological processes, carbonate biomineralization and can be used for fundamental science (as a paleoenvironmental indicator) and industry (for removal of hazardous anions). Despite a great number of works, the conditions preferable for MHC formation / stabilisation and MHC crystal chemical patterns in relation to Mg and H_2O are not clarified yet. In the course of current work, we conducted 38 syntheses to obtain information on MHC formation at different Mg/Ca ratios (0–12), pH (~9–12) and temperature (23 and 3 °C). Newly-formed carbonate precipitates were studied by means of X-ray powder diffraction, optical and scanning electron microscopy, energy dispersive X-ray spectroscopy, Raman and Fourier-transform infrared (FTIR) spectroscopies. Phase diagram for MHC, calcite, aragonite and dypingite as a function of pH and Mg concentration in solution at T= 23 °C and Ca/CO_3=0.5 was obtained. We demonstrated that MHC could be stable in dry conditions for up to two years and that the time of crystallisation is important for ACC transformation to MHC. Our results on synthetic MHC stability show that the widespread idea that MHC is a short-lived intermediate phase is wrong. For the first time, on the basis of a regular change in the unit cell parameters the possibility of significant incorporation of magnesium in MHC has been proven. According to FTIR data, it is shown to be accompanied by an increase in the water content, which leads to multidirectional change in *a* and *c* MHC parameters.

Keywords: Monohydrocalcite, Aragonite, Dypingite, Amorphous Ca carbonate, Phase diagram, Mg/Ca

INTRODUCTION

Calcium carbonate monohydrate ($CaCO_3 \cdot H_2O$) - monohydrocalcite (MHC) is the mineral, which plays an important role in many geological processes (e.g., Bischoff et al. 1991; Rodriguez-Blanco et al. 2014; Wang et al. 2015), takes an active part in carbonate biomineralization (e.g., Carlstrom 1963; Rivadeneyra et al. 2004; Lin et al. 2018) and could be effectively used for environmental contaminants sorption (e.g., Yagi and Fukushi 2012; Munemoto et al. 2014; Fukushi et al. 2017).

MHC was first reported in 1930 (Krauss and Schriever 1930) and it was described as a new mineral from sediments of Issyk Kul Lake, Kyrgyzstan in 1964 (Semenov 1964). This mineral was found in speleothems (e.g., Fischbeck and Muller 1971; Polyak et al. 1994; Onac 2001), lake sediments (e.g., Taylor 1975; Bischoff et al. 1991; Li et al. 2008) and on the surface of artificial fountains (Vereshchagin et al. 2018).

The published data highlight the importance of Mg in the formation of MHC (e.g., Sapozhnikov and Tsvetkov 1959; Last et al. 2010; Fukushi et al. 2017), even though several works showed possibility of MHC formation in Mg-free solutions (e.g., Zhang et al. 2015, 2018; González-López et al. 2018).

There are many uncertainties about magnesium incorporation in MHC. Numerous studies pointed out that natural and synthetic MHC contains magnesium, which indicates the possible $Mg^{2+} \rightarrow Ca^{2+}$ substitution. The Mg / Ca ratio in natural MHCs ranges from 0.007 to 0.45 (e.g., Sapozhnikov and Tsvetkov 1959; Stoffers and Fischbeck 1974; Taylor 1975; Dahl and Buchardt 2006; Last et al. 2010), and in synthetic MHCs from 0.005 to 0.40 (e.g., Neumann and Epple 2007; Nishiyama et al. 2013; Rodriguez-Blanco et al. 2014; Wang et al. 2015). Fukushi et al. (2017) and Fukushi and Matsumiya (2018) demonstrated that the solid solubility of Mg in the MHC structure is limited and amorphous Mg carbonate (AMC) plays an important role in Mg specialization during MHC formation. Mg-XANES spectra of MHC

with different Mg/Ca ratios revealed that the Mg in MHC is a mixture of AMC, Mg containing phase and Mg-enriched MHC (Mg/Ca ratio up to 0.06; Fukushi et al. 2017). Recent studies (Kitajima et al. 2020) based on MHC XANES spectra confirmed that Mg could be structurally incorporated in MHC (Mg/Ca ratio up to 0.4). It was also shown, that MHC synthesized at low temperature (5 ˚C) contains little Mg (Mg/Ca ratio < 0.01) and almost no AMC (Kitajima et al. 2020). In contrast, Nishiyama et al. (2013) assumed that any Mg content measured in MHC can be due to discrete Mg carbonate phase.

Rodriguez-Blanco et al. (2014) evaluated the MHC unit cell parameters during crystallization. Though the in-depth study of the structural changes in MHC as a function of Mg content were out of the scope of their study, they suggested that the observed intensive changes in unit cell parameters are connected with the expulsion of Mg from MHC into the solution. Makovicky (2017) suggested that the decrease in *a* parameter observed by Rodriguez-Blanco et al. (2014) is associated with removal misfits in MHC structure and increasing the volume of well-ordered domains. An increase in *c* parameter was explained by the decrease of the amount of magnesium in MHC (Makovicky 2017).

It was established that MHC contains 1 H_2O molecule per formula unit (Swainson 2008). However, water molecules could be incorporated into the MHC lattice in some "parasitic" manner simultaneously with Mg ions (e.g., Debuyst et al. 1993; Rodriguez-Blanco et al. 2014) as Ca and Mg ions have different hydration properties (e.g., Ikeda et al. 2007). Recently Zou et al. (2019) showed the presence of a hydrated carbonate phase ($Ca(CO_3)\cdot½H2O$), which precipitates instead of monohydrocalcite from Mg-containing solutions, if a part of magnesium (~ 2 at.%) leaves the precipitate into solution, which indicates a direct correlation between the magnesium content in crystalline calcium carbonate hydrate and the amount of water in it.

MHC is metastable with respect to calcite and aragonite at all pressures and temperatures (e.g., Hull and Turnbull 1973). Currently, there is a significant discrepancy in the assessment of the time period after which the MHC dehydration occurs. It is known that synthetic MHC can transform to aragonite in solution in 0.5–4 hours (Konrad et al. 2018), or it can dehydrate to aragonite in air in several days (Brooks et al. 1950) or a month (Kamiya et al. 1977). The age of natural MHC varies significantly: ~ 150 years in East Basin Lake (Last 1992), ~2000 years in Nam Co Lake (Li et al. 2008), and ~ 2700 years in Organic Lake (Bird et al. 1991). The deepest MHC layer in the sediments of Lake Kivu is ~ 10000 years (Stoffers and Fischbeck 1974) and in Lake Hovsgol ~ 800000 years (Solotchina et al. 2009). It is also worth noting, that the patterns of the formation of complex natural mineral carbonate assemblages, in which MHC was found, also require additional research.

Thus, the discussion of available data allows us to conclude that magnesium contribution in MHC formation and the pattern of magnesium incorporation in MHC need clarification. The objective of the present work was to synthesize MHC in various conditions (Mg/Ca ratio, pH and temperature), to characterize in detail the phase and elemental composition of the obtained precipitates, and on this basis to build a phase diagram for MHC as a function of Mg/Ca ratio and pH in solution; to specify factors affecting MHC formation and clarify the patterns of magnesium incorporation in MHC.

MATERIALS AND METHODS

Synthesis

MHC was synthesized by precipitation from aqueous solutions by the rapid addition (under constant and vigorous stirring) of $CaCl_2$ (99%, Vekton) / $MgCl_2$ $6H_2O$ (99%, Vekton) solution to a 20 mM Na_2CO_3 (99%, Vekton) / $NaHCO_3$ (99%, Vekton) / NaOH (99%, Vekton) solution. The Na_2CO_3 / $NaHCO_3$ / NaOH ratio was used to change the pH of solution. Ca/CO_3 ratio was set as 0.5 (Table 1). Two series of synthesis were performed at different temperatures and close pH values: 32 syntheses at a temperature of 23 °C (Mg/Ca 0–

12, pH 9.4–11.8; No. 1–32, Table 1) and 6 syntheses at a temperature of 3 °C (Mg/Ca 1–4, pH 9.3–10.7; No. 33–38, Table 1). Using different temperatures allowed us to compare MHC with relatively low and high amount of AMC (Kitajima et al. 2020). Syntheses were conducted for 6-35 days (No 17 and No 1, Table 1, respectively) and were stopped as the mother solution became clear and crystals formed a layer on the bottom of the beaker. The resulting precipitates were filtered, washed with deionized water several times and dried in the air for 12 hours. Precipitates, which contain MHC (No 9, 14, 18, 19, 21, 23, 26, 27, 29, 30, 31, 35, 38; Table 1, 2), were a subject for ageing experiments: a part of the material was separated and stored in a dry place at a temperature of 23 °C for a period of up to two years (730 days) and re-investigated.

Characterization methods

The resulting precipitates (after washing and drying) were studied by optical microscopy, followed by X-ray powder diffraction (PXRD) and Fourier transform infrared spectroscopy (FTIR). After that, precipitates were studied by scanning electron microscopy and energy-dispersive X-ray spectroscopy (SEM EDX). Raman spectra of different carbonates were collected on the last stage.

Optical microscopy

The morphology and optical properties of the synthesized products were studied using a Leica DM 2500P polarising light microscope.

PXRD

PXRD was used to identify the phase composition of the precipitation and determine unit cell parameters (u.c.p.) of newly-formed phases. PXRD patterns of samples were recorded on a Rigaku Miniflex II diffractometer, CuKα radiation (2-theta range 5–80°, velocity 2 °/min, step size 0.02°, Bragg-Brentano geometry). Phase identification was carried out using the PDF-2 Database. Uncertainty in the determination of magnesium carbonate,

dypingite, due to the lack of indexed X-ray patterns in the database was successfully overcome by the indexation of the corresponding diffraction reflections using u.c.p. according to Gaines et al. (1997) (Table S1). Subsequent quantitative phase content analyses of precipitates were carried out by the full-profile method using a Bruker TOPAS v. 5.0 software. R-factors (R_{wp}) were 3–10%. To check newly-formed phase stability, XRD patterns of MHC-bearing samples were recorded three times: immediately after drying, after one month (30 days) and after two years (730 days). MHC-enriched (> 90 % MHC) samples, which were obtained at different Mg/Ca ratio, pH and temperatures were used for u.c.p. determination (No 9, 14, 18, 19, 21, 23, 26, 27, 29, 31, 35, 38; Table 1, 2). Unit cell parameters were determined by a Rigaku Ultima IV high resolution diffractometer, CuKα radiation (2-theta range 5–120°, velocity 1 °/min, step size 0.02 °, Bragg-Brentano geometry; PSD D-Tex Ultra detector) with internal standard (Ge). MHC u.c.p. were calculated based on 11 peaks (hkl: 031, 221, 032, 222, 141, 060, 061, 251, 144, 442, 361), which were not overlaid by Ge. In order to detect the phase composition of MHC spheres they were studied by a Rigaku R-AXIS Rapid II diffractometer equipped with a curved (cylindrical) imaging plate detector (r = 127.4 mm), Co$K\alpha$ radiation; exposure time was set to 20 min. The obtained data were processed using osc2xrd program (Britvin et al. 2017).

Vibrational spectroscopy

To verify the phase composition of the obtained precipitates and check the possible variations of water content in MHC a Raman and FTIR spectroscopy were used**.**

Raman spectra of morphologically different grains (which were found by optical microscopy) were recorded by a Horiba Jobin-Yvon LabRAM HR800 spectrometer equipped with a microscope (Olympus). The microscope is equipped with 50x and 100x objectives. Raman spectra were excited by an Ar ion laser at wavelengths of 488 and 514 nm and a maximum power of 50 mW. The spectra were obtained in the range of 100–4000 cm^{-1} at a

resolution of 2 cm^{-1} and at room temperature. To improve the signal-to-noise ratio the number of acquisitions was set to 20. The spectra were processed using licensed Labspec and Origin software.

FTIR spectra of MHC-enriched (> 90 % MHC) samples (No 9, 18, 21, 27, 31; Table 1) were recorded by a Bruker Vertex 70 within the scanning range of 400–4000 cm^{-1} with a resolution of 4 cm^{-1}. In order to estimate the variations in H_2O content, the resulted spectra were normalised on 873 cm^{-1} carbonate line of MHC (Neumann and Epple 2007) as it was assumed that the content of the carbonate ion did not change from sample to sample.

SEM EDX

The morphology and chemical composition of newly-formed phases were studied by means of a Hitachi S-3400 N SEM equipped with an Oxford Instruments AzTec Energy X-Max 20 EDX spectrometer, with the following parameters: 20 kV accelerating voltage, 1 nA beam current and 30 s data-collection time (excluding dead time).

The magnesium content in the carbonate phases was determined semi-quantitatively as (1) the samples have not been polished (in order to preserve them from heating and the influence of chemical reagents) and (2) synthesized carbonates formed the intergrowths that were much smaller than the typical EDX spot (~1 μm).

RESULTS

X-ray powder diffraction

According to PXRD, the obtained precipitates consist of MHC, calcite, aragonite and dypingite, which were formed in different ratios (Figure 1, Table 2). Phase composition depends on Mg/Ca ratio in solution, pH and temperature. Comparison of the PXRD patterns of precipitates synthesized at different temperatures but at the same Mg/Ca ratio and pH (9 and 35; 18 and 38; Table 2) showed that at 3 °C aragonite and calcite (which were present at room temperature) disappear and only MHC is formed. Besides that, we observed that

synthetic carbonates, which were formed in the upper part of the beaker, are aragonite-enriched, whereas precipitates formed on the bottom contain smaller amounts of aragonite or none. Due to that, it was possible to separate almost pure MHC for u.c.p. and FTIR investigations.

MHC did not show any changes after exposure in air for 30 and 730 days (Figure 1a, b). Neither peak broadening nor the appearance of new peaks was found. The same observation was made for calcite, aragonite and dypingite (Figure 1b, c). MHCs spheres obtained from solution with different Mg/Ca ratio (Mg/Ca 1-9) have the same PXRD patterns (Figure 1d).

Both *a* and *c* parameters of MHC from different syntheses change significantly with the increase of the Mg content in solution (initial): *a* decreases from 10.564 to 10.554 Å, *c* increases from 7.501 to 7.522 Å (Table 2; Figure 2). The u.c.p. of MHC obtained at different temperatures but at the same Mg/Ca ratio in solution and pH (No 9 and 35; 18 and 38; Table 2) have the same values within an error (Table 2). The dimensions of coherent scattering domains (CSD) vary insignificantly (from 28 to 62 nm, Table 2).

MHC precipitated from carbonate solutions at the range of initial pH values from 9.7 to 10.5 and with the obligatory presence of magnesium cations in the solution (Mg/Ca 0.5-12.0; Table 2). MHC was not observed in the absence of magnesium cations, as well as at initial pH values of solutions of less than 9.7. At 23 °C MHC was obtained in 17 out of 32 experiments (Table 2) and at 3 °C in 4 out of 6 experiments (Table 2). Based on PXRD, MHC formed as a single phase in 6 experiments (No 17, 26, 29, 31, 35, 38; Table 2), precipitated with aragonite in 13 experiments (No 9, 13, 14, 18, 19, 21, 22, 23, 25, 27, 36, 37; Table 2), with calcite - in 3 experiments (No 9, 36, 37; Table 2), with dypingite - in 3 experiments (No 22, 30, 32; Table 2).

Aragonite was found in most of Mg-bearing syntheses (Mg/Ca>0.5; Table 1, 2). Aragonite tends to be the main phase in carbonate assemblages with initial pH < 10.5. There is a significant increase in the amount of crystallized aragonite compared to calcite with an increase in the Mg/Ca ratio in the initial solution (Table 2). As indicated above, aragonite tends to form on the upper boundary water/air.

Calcite was found both in Mg-free and Mg-bearing syntheses. Only calcite precipitates if Mg/Ca ≤0.5 and initial pH ranges from 9.3 up to 11.7 (Table 2). In Mg-bearing synthesis calcite crystallises in Mg/Ca ratio 0.5-10. Calcite mainly formed on the bottom of the beaker.

Dypingite precipitated from the solution with high magnesium content (Mg/Ca= 6-12) and high pH (pH start >10.6). However, as very high pH could be hardly obtained in synthesis simultaneously with high Mg/Ca ratio, it is hard to discuss the influence of these factors.

Vibrational spectroscopy

The obtained Raman spectra (Figure 3) are typical for MHC (e.g., Coleyshaw et al. 2003), calcite (e.g., Tomić et al. 2010), aragonite (e.g., Tomić et al. 2010), and dypingite (Frost et al. 2009). So Raman spectroscopy study confirmed PXRD data on the phase composition of precipitates, which was important in the case of dypingite. The following Raman bands were recorded: MHC (Coleyshaw et al. 2003) – 693 ($\nu_4(CO_3)^{2-}$), 718 ($\nu_4(CO_3)^{2-}$), 871 ($\nu_2(CO_3)^{2-}$), 1065 ($\nu_1(CO_3)^{2-}$) cm^{-1}; calcite (Tomić et al. 2010) – 151 (lattice vibrations), 278 (lattice vibrations), 710 ($\nu_4(CO_3)^{2-}$), 1085 ($\nu_1(CO_3)^{2-}$) cm^{-1}; aragonite (Tomić et al. 2010) – 149 (lattice vibrations), 199 (lattice vibrations), 700 ($\nu_4(CO_3)^{2-}$), 704 ($\nu_4(CO_3)^{2-}$), 1082 ($\nu_1(CO_3)^{2-}$) cm^{-1}, dypingite (Tomić et al. 2010) – 727 ($\nu_2(CO_3)^{2-}$), 761 ($\nu_2(CO_3)^{2-}$), 1092 ($\nu_1(CO_3)^{2-}$), 1120 ($\nu_1(CO_3)^{2-}$), 1450 ($\nu_3(CO_3)^{2-}$), 1587 ($\nu_1(CO_3)^{2-}$), 3422 ($\nu(OH)^-$), 3514 ($\nu(OH)^-$), 3647($\nu(OH)^-$). Dypingite was studied by Raman spectroscopy both in dypingite-rich samples (No 22, 30, 32; Table 2), and dypingite-poor samples, where it was

detected by SEM-EDX (see below). Due to the intense luminescence it was not possible to study OH-region of MHC by Raman spectroscopy.

FTIR spectra of precipitates, obtained from solutions with different Mg/Ca ratio (No 9, 18, 21, 27, 31; Table 1) are typical for MHC (Neumann and Epple 2007; Senorale-Pose et al. 2008; Kimura and Koga 2011; Wang et al. 2015). The following bands were distinguished: 589 (lattice), 700 ($\nu_4(CO_3^{2-})$), 765 (lattice*)*, 873 ($\nu_2(CO_3)^{2-}$), 1068 ($\nu_1(CO_3)^{2-}$), 1411/1490 ($\nu_3(CO_3)^{2-}$), 1703 (H_2O deformation), 2800–3700 (H_2O, stretch) (Figure 4a). A broad line, characteristic of dypingite (but not for MHC), in the region of 947-1000 cm^{-1} (Hopkinson et al. 2008; Frost et al. 2009) is absent on the FTIR spectra of the studied samples, which is in good agreement with the PXRD data on the absence of dypingite in these samples. As we did not observe both amorphous calcium carbonate (ACC) or amorphous magnesium carbonate (AMC) in precipitates, we can conclude that the integral intensity of the broad line ~ 2800–3700 cm^{-1} on the FTIR spectra of the studied samples characterizes the water content in MHC. There is a trend level direct correlation between the water content in MHCs (defined in this way) and Mg/Ca ratios in solution (Figure 4b) and, accordingly, a trend level correlations between the water content in MHCs and its u.c.p.

Scanning electron microscopy and energy-dispersive X-ray spectroscopy

According to EDX data, the composition of MHC spheres includes magnesium, the amount of which varies significantly (from 1 to 18 wt.% MgO). Elemental mapping of MgKα and CaKα in MHC sphere (Figure 5) showed that Mg-enriched local areas are associated with interstices, in which Mg-enriched inclusions are likely to be present. Some authors (e.g. Zhang et al., 2015) mention core-to-border variations in chemical composition of MHC and explained it by stabilizing effects of “impurities”. However, in our case we did not observe such a “borders” in studied spheres (Mg content was almost the same in the border regions). Based on our XRD and Raman results we can assume that these inclusions are rather small

dypingite particles than relicts of AMC (Fukushi et al. 2017). MHC aggregates are bluish and translucent under optical observation with a distinct opal tint. MHC forms spheres (Figure 6a-c), which according to PXRD are typically homogeneous (Figure 1d) and are composed of thin cone-shaped fibers, tightly adjacent to each other (Figure 6d). The thickness of the fibers varies from a few nanometers at the beginning of their growth (at the center of the sphere) to several microns at the end of the growth (on the surface of the sphere). Each of the sub-individuals ends up on the spherule surface with a trigonal pyramid (Figure 6d).

Calcite showed wide variability in Mg content (up to 18 wt. % MgO; Figure 7a). The Mg/Ca ratio in calcite approached 1 as the Mg content in solution increased. At the same time, XRD peaks became broader and shifted to higher 2-theta. Calcite micromorphology is strongly influenced by pH and Mg/Ca ratio. Calcite forms rhombohedral crystals up to 8 μm in size, having smooth edges and a smooth faceting in Mg-free solution despite initial pH. At low pH (pH <9), its edges became spikier compared to calcite from Mg-free synthesis. If pH increased further on (pH 9-10) calcite started to form dumbbell-like crystals. Calcite crystals became spheres if pH exceeded 10.

Aragonite is magnesium free (Figure 7b). Aragonite crystallizes in the shape of needle-like crystals, forming either dumbbell-like aggregates or spheres (Figure 6b, c). The growth of aragonite needle crystals on MHC spherules (Figure 6c) indicates aragonite formation on the later stages of crystallization (compared with MHC).

According to EDX data the calcium-free magnesium phase (Figure 7c) is present in subordinate amount in all syntheses, where MHC was found. Based on PXRD and Raman spectroscopy data we can propose that this phase is dypingite. SEM images show that dypingite forms spheres composed of very thin perforated crystal plates (Figure 6c). Dypingite from dypingite-enriched synthesis (No 22, 30, 32; Table 2) has more smooth faces and is more amorphous-like.

DISCUSSION

Monohydrocalcite formation conditions

According to most of the previous studies, MHC forms *via* ACC or AMC (e.g., Rodriguez-Blanco et al. 2014; Wang et al. 2015). We did not find ACC / AMC in precipitates, obtained both at high- and low-temperatures. However, we observed that mother solution looks milky for 5-20 days. As no *in situ* PXRD studies have been done in mother solution, we can propose that ACC/AMC exist on initial stages of precipitate synthesis, but are later transformed into crystalline phases. Previously Fukushi and Matsumiya (2018) demonstrated that a reaction time of 24 h was insufficient to reach equilibrium in MHC synthesis. So we can assume that the lack of amorphous phase in precipitates obtained in our experiments is due to the use of long exposure experiments (7-35 days) during which an almost complete transformation of ACC into crystalline phases was achieved. This assumption is supported by the size of MHC spherules (which are relatively big - up to 400 μm - and well crystallized) (Figure 5, 6).

The results of a detailed study of obtained precipitates allowed us to establish the pattern of carbonate formation as a function of Mg/Ca ratio (starting value in solution) and pH at T= 23 °C and Ca/CO_3=0.5 (Figure 8a-b).

Four fields could be distinguished on the Mg/Ca – pH_{start} plot (solid fill; Figure 8a): (I) pure calcite (green, Mg/Ca=0, pH 9.3-11.8), (II) calcite with aragonite (orange, IIa: Mg/Ca 0.5-10, pH 9.6-10.1 and IIb: Mg/Ca 1, pH 11-11.6), (III) MHC with aragonite (violet, Mg/Ca 0.5-12, pH 10.1 – 10.7), (IV) MHC with dypingite (lilac, Mg/Ca 6-12, pH 10.5-10.7).

In the process of the crystallization of carbonates, a change occurs in the pH of the solutions (Table 1). The pH value could be shifted both to low and higher numbers of up to 1.3 from its initial state. During the crystallization of MHC, the pH increases by 0.10–0.30. On the contrary, during the crystallization of calcite and aragonite, the pH value decreases by

0.03–0.40. Indeed, writing the chemical reactions of mineral formation suggest that pH should decrease in all cases. However, we think that the reactions may not cover the complexity of the crystallisation process, which proceeds in several stages and through the amorphous phase(s) (e.g. e.g. Nishiyama et al. 2013; Rodriguez-Blanco et al. 2014).

As a result, the field boundaries are shifted and Mg/Ca – pH_{finish} plot is different (dashed fill; Figure 8b). Three fields could be distinguished (Figure 8b): (I) pure calcite (green, Mg/Ca=0, pH 9.5-11.7), (II) calcite with aragonite (orange, IIa: Mg/Ca 0.5-10, pH 9.5-10.4 and IIb: Mg/Ca 1, pH 11.2), (III) MHC with aragonite and dypingite (violet, Mg/Ca 0.5-12, pH 9.7-11).

MHCs formation requires calcite nucleation inhibiting. It is known that divalent cations such as magnesium could inhibit calcite nucleation (e.g., Mucci et al. 1989; Nielsen et al. 2016; Tollefsen et al. 2018). If no magnesium was added to the solution, only calcite precipitates, which explains the presence of the field No I (Figure 8a, b). The pH contribution is not so straightforward. According to Tollefsen et al. (2018) higher pH values also inhibits calcite nucleation, which leads to aragonite, ikaite or MHC precipitation. It was found that higher CO_3 concentration could be obtained at higher pH (Hu et al. 2014) and as a result, different supersaturation of aragonite / MHC could be obtained at different pH. That could be an explanation for the fields No II-III on the diagram (Figure 8a-b). According to Konrad et al. (2016), polymorph formation from ACC also depends on the physicochemical boundary conditions during transformation, which could explain different amount of aragonite in upper and lower parts of the beaker. Our data allowed to establish the field of dypingite (field IV). Previously, dypingite along with nesquehonite was successfully synthesised from AMC (e.g., Tanaka et al. 2019), but it was rarely reported in assemblage with natural/synthetic MHC (e.g., Dahl and Buchardt 2006). In most works hydromagnesite (e.g., Rodriguez-Blanco et al. 2014; Pan et al. 2019), nesquehonite (e.g., Fischbeck and Muller 1971) or other hydrous Mg

carbonates (e.g., Nishiyama et al. 2013; Fukushi et al. 2017) are considered to be the main Mg-phase concomitant to MHC. There could be several reasons for such a discrepancy. First of all, previous studies have showed that hydrous magnesium carbonates could transform to each other (e.g., Ballirano et al. 2013; Montes-Hernandez and Renard 2016; Harrison et al. 2018), and final carbonate assemblage would contain the most stable phase. Second, $Ca:CO_3$ ratio is one of the factors controlling carbonate formation (e.g., Rodriguez-Blanco et al. 2014) and for this reason the formation of dypingite instead of hydromagnesite could be the result of $Ca:CO_3$ ratio used (0.5 (our data) instead of ~0.7 (Rodriguez-Blanco et al. 2014)). Third, dypingite could be overlooked as (1) there are no structural data and reliable PXRD patterns and (2) dypingite amount in the precipitate is very small and could not be detected by PXRD in most of the cases (see PXRD and SEM EDX sections).

Our data confirmed that low temperatures are favourable for MHC formation (Table 2). Comparison of the PXRD results of synthesis provided at different temperatures but at the same Mg/Ca ratio and pH (9 and 35; 18 and 38; Table 2) showed, MHC at low temperature becomes more stable than aragonite. This observation in consistency with Kitajima et al. (2020), who showed preferable MHC formation at low temperature. Moreover, we can suggest that relative abundance of MHC in Ikka Fjord (e.g., Dahl and Buchardt 2006) and caves (e.g., Onac 2001) is also due to the low temperature during its formation. We did not find any relation between dypingite amount and temperature conditions.

As was described above, MHC synthesized at various magnesium contents in solution (Mg/Ca = 1-12, Table 2) does not show any changes after exposure in dry state for up to 730 days (2 years). This result indicates that MHC stability in dry conditions caused by strong bonding between water molecules and other structure units, which makes dehydration an energetically disadvantageous process. Each water molecule connects with two $(CO_3)^{2-}$groups in the MHC structure by hydrogen bonds (Swainson 2008; Figure 9a) and cannot readily

diffuse out. This idea is in good agreement with Chaka's data (2019), according to which the hydration of MHC and its conversion to calcite, aragonite or vaterite occurs through dissolution and subsequent precipitation.

Mg^{2+} –ions incorporation in monohydrocalcite

The crystal structure of MHC (sp.gr $P3_1$) was determined using X-ray single crystal data by Effenberger (1981) and refined on the base of neutron and X-ray powder diffraction data by Swainson (2008). According to Swainson (2008) Ca atoms are eight-coordinated in MHC structure (Figure 9a). Ca atoms, CO_3 groups and water molecules form «rods» along [001] in which a spiral arrangement of Ca ions is accompanied by spiral arrangements of CO_3 groups and of H_2O molecules (Figure 9a, b). Makovicky (2017) estimated the order–disorder potential of the MHC crystal structure. He showed that the ordered MHC structure is a complicated periodic arrangement containing rods of two opposite orientations. However, various degrees of rod distribution disorder should occur, generating only small energy penalty.

The observed changes of u.c.p. of MHC along with an increase of Mg content in solution clearly support that the composition of MHC changes with increasing magnesium concentration in the precipitate. Of course, not all the magnesium appearing in the precipitate was incorporated in MHC and replaced calcium. The presence of calcite, aragonite and dypingite in precipitates could lead to a slight reduction of magnesium content in MHC. However, the effect of these phases on the redistribution of magnesium in precipitates and MHC u.c.p. was very neglectable, since: (a) aragonite contains no Mg, (2) calcite was found in subordinate amount and only in 1 sample used for u.c.p. determination (No. 9, Table 2), (3) dypingite and ACC/AMC were absent on PXRD.

The observed significant inverse correlation between *a* parameter and the Mg / Ca ratio in the solution (Figure 2) reliably confirms that as magnesium content in solution

increases, the magnesium content in MHC increases as well. Parameter *a* decreases due to $Mg^{2+} \rightarrow Ca^{2+}$ substitution (r^{VIII}_{Mg}=0.89 Å< r^{VIII}_{Ca}=1.12 Å; Shannon 1976). One cannot exclude a small contribution to the reduction of *a* parameter by misfits in MHC structure (Makovicky 2017), they occur due to the irregular distribution of parallel to [001] "rods" (Figure 9a, b). It can be assumed that an increase of disorder in "rod" distribution may be associated with an increase of disorder in Mg distribution as Mg content in MHC changes.

The direct correlation between the values of *c* parameter of MHC and Mg/Ca ratio in mother solution (Figure 2b) can be explained by the simultaneous incorporation of water molecules and Mg ions into the MHC lattice (e.g., Debuyst et al. 1993). Such an assumption is in agreement with FTIR data: as Mg content in solution increases, the amount of H_2O in MHC also increases (Figure 4b). A number of published experimental works also confirms this idea (Ihli et al. 2014; Rodriguez-Blanco et al. 2014; Zou et al. 2019). The structural mechanism leading to the prevailing Mg effect on *a* parameter and water effect on *c* parameter, needs further clarification.

Unit cell parameters of synthetic MHC, obtained from solutions at various Mg/Ca ratio are close to each other (*a* 10.564-10.554, *c* 7.501- 7.522 Å (our data); *a* 10.539-10.520, *c* 7.501- 7.527 Å (Rodriguez-Blanco et al. 2014)) and to the published data on natural MHC (*a* 10.555, c 7.564 Å; Swainson 2008; Figure 10). Higher values of *a* parameter in our samples (in comparison with Rodriguez-Blanco et al. 2014) are well explained by the lower content of magnesium in our MHC. The values of the *c* parameter of the MHC in both experiments are very close, but MHCs synthesised by Rodriguez-Blanco et al. (2014) have a wider range of variations in the *c* parameter, and hence, according to our model, they have a wider range of variations in water content. The maximum value of *c* parameter of MHC synthesized by Rodriguez-Blanco et al. (2014) is 7×10^{-3} Å higher than in the MHC obtained by us (Mg / Ca = 12; No 31; Table 2), which is well explained by the high water content in it.

The *a* parameter of natural MHC studied by Swainson (2008) is similar to the *a* parameter of MHC synthesized by us at Mg / Ca = 12 (No 31; Table 2), whereas the *c* parameter is significantly higher than that of all synthetic MHCs (Figure 10). This suggests that Mg-content in natural MHC is almost the same as in the MHC synthesized by us from a solution with Mg/Ca = 12, while the water content in the natural sample is higher. According to structural data (Swainson 2008) the number of water molecules in the studied MHC is close to 1, i.e. corresponds to the maximum possible value (for this structural model). Values of u.c.p. of Mg-free and Mg-bearing MHC calculated *via* density-functional theory and ab initio thermodynamics approaches (Fukushi and Matsumiya 2018; Chaka 2019) vary greatly and differ significantly from the experimentally determined u.c.p values. It allows us to suggest that the structural models used in the calculations were far enough from the real MHC crystal structure.

As regarded above, the u.c.p. values obtained by Rodriguez-Blanco et al. (2014) and the direction of their changes were almost similar to those we observed. But unlike us, Rodriguez-Blanco et al. (2014) detected an intense change in the parameters after the formation of MHC with *a* 10.519 and *c* 7.501 Å, with 0.26 Mg atoms per formula unit (apfu). Unlike us, the authors explained the changes in u.c.p. at this later stage by a gradual decrease in the magnesium content in MHC due to the formation of hydromagnesite. We think that such an explanation would be valid if the changes in u.c.p. slowed down or the direction of their changes inversed. However, neither of these processes was observed (Rodriguez-Blanco et al. 2014).

Our results show that the Mg content in MHC spheres reaches 18 wt.% MgO which is slightly lower to earlier obtained values (e.g., Rodriguez-Blanco et al. 2014). So our data along with the data of Rodriguez-Blanco et al. (2014) contradict the results of Fukushi and Matsumiya (2018) and show that MHC could contain sufficient amounts of Mg. In addition,

the relation between MHC u.c.p. and magnesium content in the precipitating solution (and its relative content in MHC, consequently,) was established for the first time. It was shown that the Mg incorporation in MHC is accompanied by the increase of water content in it.

Based on our results and previously published data, we suggest that the real composition of MHC corresponds to the following formula: $(Ca_{1-x}Mg_x)(CO_3)\ yH_2O$, $y \leq 1$ (structural constraint, Swainson 2008). The maximum x value in the results of different authors diverges significantly (but as stated above, not less than 0.26 apfu (Rodriguez-Blanco et al. 2014)) and requires further investigation.

IMPLICATIONS

The present work contributes to mineralogy of hydrated calcium and magnesium carbonates—minerals, which play an important role in many geological processes, take an active part in carbonate biomineralization and are efficiently used for the sorption of environmental contaminants.

Phase diagrams (at 23 ºC and Ca/CO_3 0.5) for MHC, calcite, aragonite and dypingite precipitation, as a function of pH and Mg/Ca ratio in solution was obtained. Our contribution towards the understanding of the chemical controls on MHC formation has implications for the understanding of MHC occurrence in nature. It is worth noting that the obtained carbonate assemblages are similar to those found in nature. In most cases, MHC associates with H_2O-free calcium carbonates, like aragonite or calcite (e.g., Fischbeck and Muller 1971; Sklyarov et al. 2010). Magnesium carbonates, such as hydromagnesite, nesquehonite, dolomite (e.g., Fischbeck and Muller 1971), dypingite (e.g., Dahl and Buchardt 2006), lansfordite (e.g., Garvie 2003) and huntite (e.g., Riedinger et al. 2002), are also commonly found in nature with MHC. A further work on the determination of the thermodynamic properties of MHCs with different Mg/Ca ratio and water content, in order to draw stability diagrams is needed.

The stability of synthetic MHC (along with calcite, aragonite and dypingite) in a dry state for up to two years was demonstrated. It was shown that elevated magnesium content, low temperatures and a long time of crystallisation are favourable for MHC formation.

For the first time, the possibility of significant incorporation of magnesium in MHC on the basis of a regular change in the unit cell parameters has been proven. It was shown that an increase in magnesium content is accompanied by an increase in water content, which leads to multidirectional change in *a* and *c* parameters in MHC.

Our results append previous findings and allow a better understanding of the naturally observed situation with the presence of MHC in deposits of different age and origin. It is notable that MHC has been found in nature at low temperature (e.g., Dahl and Buchardt 2006) and MHC of Lake Hovsgol was found in glacial-type sediments (Solotchina et al. 2009). We can assume that "metastable" MHC has been preserved in 800,000 year-old (Solotchina et al. 2009) sediments, not just because of the low temperature and increased phosphorus content (Lin et al. 2018), but also due to the low availability of water, which was removed from the sediments. In addition, such results for MHC stability show that the widespread idea that MHC is a short-lived intermediate phase is wrong.

ACKNOWLEDGEMENTS

We are grateful to Vladimir N. Bocharov for performing the Raman analysis. This research was supported by the Russian Science Foundation (Grant 19-17-00141). The authors thank the X-ray Diffraction Centre and “Geomodel” Resource Centre of Saint-Petersburg State University for providing instrumental and computational resources.

REFERENCES LIST

Ballirano, P., De Vito, C., Mignardi, S., and Ferrini, V. (2013) Phase transitions in the Mg-CO_2-H_2O system and the thermal decomposition of dypingite, $Mg_5(CO_3)_4(OH)_2 \cdot 5H_2O$: Implications for geosequestration of carbon dioxide. Chemical Geology, 340, 59–67.

Bird, M.I., Chivas, A.R., Radnell, C.J., and Burton, H.R. (1991) Sedimentological and stable-isotope evolution of lakes in the Vestfold Hills, Antarctica. Palaeogeography, Palaeoclimatology, Palaeoecology, 84, 109–130.

Bischoff, J.L., Herbst, D.B., and Rosenbauer, R.J. (1991) Gaylussite formation at mono lake, california. Geochimica et Cosmochimica Acta, 55, 1743–1747.

Britvin, S.N., Dolivo-Dobrovolsky, D. V., and Krzhizhanovskaya, M.G. (2017) Software for processing the X-ray powder diffraction data obtained from the curved image plate detector of Rigaku RAXIS Rapid II diffractometer. Proceedinga of Russian Mineralogical Society, 146, 104–107.

Brooks, R., Clark, L.M., and Thurston, E.F. (1950) Calcium Carbonate and Its Hydrates. Philosophical Transactions of the Royal Society A: Mathematical, Physical and Engineering Sciences, 243, 145–167.

Carlstrom, D. (1963) A crystallographic study of vertebrate otoliths. Biological Bulletin, 125, 441–462.

Chaka, A.M. (2019) Quantifying the Impact of Magnesium on the Stability and Water Binding Energy of Hydrated Calcium Carbonates by Ab Initio Thermodynamics. Journal of Physical Chemistry A, 123, 2908–2923.

Coleyshaw, E.E., Crump, G., and Griffith, W.P. (2003) Vibrational spectra of the hydrated carbonate minerals ikaite , monohydrocalcite , lansfordite and nesquehonite. Spectrochimica Acta Part A, 59, 2231–2239.

Dahl, K., and Buchardt, B. (2006) Monohydrocalcite in the Arctic Ikka Fjord, SW Greenland: First Reported Marine Occurrence. Journal of Sedimentary Research, 76, 460–471.

Debuyst, R., Deiehet, F., and Idrissi, S. (1993) Paramagnetic Centers in y-Irradiated Synthetic Monohydrocalcite. Applied Radiation and Isotopes, 44, 293–297.

Effenberger, H. (1981) Crystal Structure and Infrared Absorption Spectrum of Synthetic Monohydrocalcite, CaCO3 H20. Monatshefte fiir Chemic, 112, 899–909.

Fischbeck, R., and Muller, G. (1971) Monohydrocalcite, hydromagnesite, nesquehonite, dolomite, aragonite and calcite in speleothems of the Frankische Schweiz, Western Germany. Contributions to Mineralogy and Petrology, 33, 87–92.

Frost, R.L., Bahfenne, S., and Graham, J. (2009) Raman spectroscopic study of the magnesiumcarbonate minerals-artinite and dypingite. Journal of Raman Spectroscopy, 40, 855–860.

Fukushi, K., and Matsumiya, H. (2018) Control of Water Chemistry in Alkaline Lakes: Solubility of Monohydrocalcite and Amorphous Magnesium Carbonate in CaCl2-MgCl2-Na2CO3 Solutions. ACS Earth and Space Chemistry, 2, 735–744.

Fukushi, K., Suzuki, Y., Kawano, J., Ohno, T., Ogawa, M., Yaji, T., and Takahashi, Y. (2017) Speciation of magnesium in monohydrocalcite: XANES, ab initio and geochemical modeling. Geochimica et Cosmochimica Acta, 213, 457–474.

Gaines, R. V, Skinner, H.C.W., Foord, E.R., Mason, B., and Rosenzweig, A. (1997) Dana's New Mineralogy: The System of Mineralogy of James Dwight Dana and Edward Salisbury Dana, 1872 p. John Wiley & Sons Inc., New York.

Garvie, L.A.J. (2003) Decay-induced biomineralization of the saguaro cactus (Carnegiea gigantea). American Mineralogist, 88, 1879–1888.

González-López, J., Fernández-González, Á., and Jiménez, A. (2018) Precipitation behaviour in the system Ca2+-Co2+-CO32−-H2O at ambient conditions — Amorphous phases and CaCO3 polymorphs. Chemical Geology, 482, 91–100.

Harrison, A.L., Mavromatis, V., Oelkers, E.H., and Bénézeth, P. (2019) Solubility of the hydrated Mg-carbonates nesquehonite and dypingite from 5 to 35°C: Implications for CO 2 storage and the relative stability of Mg-carbonates. Chemical Geology, 504.

Hopkinson, L., Rutt, K., and Cressey, G. (2008) The transformation of nesquehonite to hydromagnesite in the system CaO-MgO-H_2O-CO_2: An experimental spectroscopic study. Journal of Geology, 116, 387–400.

Hu, Y. Bin, Wolf-Gladrow, D.A., Dieckmann, G.S., Völker, C., and Nehrke, G. (2014) A

laboratory study of ikaite ($CaCO_3 \cdot 6H_2O$) precipitation as a function of pH, salinity, temperature and phosphate concentration. Marine Chemistry, 162, 10–18.

Hull, H., and Turnbull, A.G. (1973) A thermochemical study of monohydrocalcite. Geochimica et Cosmochimica Acta, 37, 685–694.

Ihli, J., Wong, W.C., Noel, E.H., Kim, Y.Y., Kulak, A.N., Christenson, H.K., Duer, M.J., and Meldrum, F.C. (2014) Dehydration and crystallization of amorphous calcium carbonate in solution and in air. Nature Communications, 5, 1–10.

Ikeda, T., Boero, M., and Terakura, K. (2007) Hydration properties of magnesium and calcium ions from constrained first principles molecular dynamics. The Journal of Chemical Physics, 127, 074503.

Kamiya, K., Sakka, S., and Terada, K. (1977) Aragonite formation through precipitation of calcium carbonate monohydrate. Materials Research Bulletin, 12, 1095–1102.

Kimura, T., and Koga, N. (2011) Monohydrocalcite in Comparison with Hydrated Amorphous Calcium Carbonate : Precipitation Condition and Thermal Behavior. Crystal Growth and Design, 11, 3877–3884.

Kitajima, T., Fukushi, K., Yoda, M., and Takeichi, Y. (2020) Simple , Reproducible Synthesis of Pure Monohydrocalcite with Low Mg Content. Minerals, 10, 1–8.

Konrad, F., Gallien, F., Gerard, D.E., and Dietzel, M. (2016) Transformation of Amorphous Calcium Carbonate in Air. Crystal Growth and Design, 16, 6310–6317.

Konrad, F., Purgstaller, B., Gallien, F., Mavromatis, V., Gane, P., and Dietzel, M. (2018) Influence of aqueous Mg concentration on the transformation of amorphous calcium carbonate. Journal of Crystal Growth, 498, 381–390.

Krauss, F., and Schriever, W.Z. (1930) Die Hydrate des Calciumcarbonats. Zeitschrift fur Anorganische und Allgemeine Chemie, 188, 259–273.

Last, F.M., Last, W.M., and Halden, N.M. (2010) Carbonate microbialites and hardgrounds from Manito Lake, an alkaline, hypersaline lake in the northern Great Plains of Canada. Sedimentary Geology, 225, 34–49.

Last, W.M. (1992) Petrology of modern carbonate hardgrounds from East Basin Lake, a saline maar lake, southern Australia. Sedimentary Geology, 81, 215–229.

Li, M., Kang, S., Zhu, L., You, Q., Zhang, Q., and Wang, J. (2008) Mineralogy and geochemistry of the Holocene lacustrine sediments in Nam Co, Tibet. Quaternary International, 187, 105–116.

Lin, C.Y., Turchyn, A. V., Steiner, Z., Bots, P., Lampronti, G.I., and Tosca, N.J. (2018) The role of microbial sulfate reduction in calcium carbonate polymorph selection. Geochimica et Cosmochimica Acta, 237, 184–204.

Makovicky, E. (2017) The order–disorder potential of the crystal structure of monohydrocalcite, CaCO3·H2O. Mineralogy and Petrology, 112, 105–109.

Montes-Hernandez, G., and Renard, F. (2016) Time-Resolved in Situ Raman Spectroscopy of the Nucleation and Growth of Siderite, Magnesite, and Calcite and Their Precursors. Crystal Growth and Design, 16, 7218–7230.

Mucci, A., Canuel, R., and Zhong, S. (1989) The solubility of calcite and aragonite in sulfate-free seawater and the seeded growth kinetics and composition of the precipitates at 25°C. Chemical Geology, 74, 309–320.

Munemoto, T., Fukushi, K., Kanzaki, Y., and Murakami, T. (2014) Redistribution of Pb during transformation of monohydrocalcite to aragonite. Chemical Geology, 387, 133–143.

Neumann, M., and Epple, M. (2007) Monohydrocalcite and Its Relationship to Hydrated Amorphous Calcium Carbonate in Biominerals. Berichte der deutschen chemischen Gesellschaft, 14, 1953–1957.

Nielsen, M.R., Sand, K.K., Rodriguez-Blanco, J.D., Bovet, N., Generosi, J., Dalby, K.N., and

Stipp, S.L.S. (2016) Inhibition of calcite growth : Combined effects of Mg and SO. Crystal Growth and Design, 16, 6199–6207.

Nishiyama, R., Munemoto, T., and Fukushi, K. (2013) Formation condition of monohydrocalcite from CaCl2-MgCl2-Na2CO3 solutions. Geochimica et Cosmochimica Acta, 100, 217–231.

Onac, B.P. (2001) Mineralogical studies and Uranium-series dating of speleothems from Scarisoara Glacier Cave (Bihor Mountains, Romania). Theoreical and Applied Karstology, 13–14, 33–38.

Pan, J., Zhao, H., Tucker, M.E., Zhou, J., Juang, M., Wang, Y., Zhao, Y., Sun, B., Han, Z., and Yan, H. (2019) Biomineralization of Monohydrocalcite Induced by the Halophile Halomonas Smyrnensis WMS-3. Minerals, 9, 632.

Polyak, V.C., Jacka, A.D., and Güven, N. (1994) Monohydrocalcite in speleothems from caves in the Guadalupe Mountains, New Mexico. National Speleological Society, Bulletin, 56, 27–31.

Riedinger, M.A., Steinitz-Kannan, M., Last, W.M., and Brenner, M. (2002) A ~6100 ^{14}C yr record of El Niño activity from the Galápagos Islands. Journal of Paleolimnology, 27, 1–7.

Rivadeneyra, M.A., Párraga, J., Delgado, R., Ramos-Cormenzana, A., and Delgado, G. (2004) Biomineralization of carbonates by Halobacillus trueperi in solid and liquid media with different salinities. FEMS Microbiology Ecology, 48, 39–46.

Rodriguez-Blanco, J.D., Shaw, S., Bots, P., Roncal-Herrero, T., and Benning, L.G. (2014) The role of Mg in the crystallization of monohydrocalcite. Geochimica et Cosmochimica Acta, 127, 204–220.

Sapozhnikov, D.G., and Tsvetkov, A.I. (1959) Precipitation of hydrous calcium carbonate on the bottom of Lake Issyk-Kul. Akadimiya Nauk SSSR, 124, 131–133.

Semenov, E.J. (1964) Hydrated carbonates of sodium and calcium. Kristallografiya, 9, 109–110.

Senorale-Pose, M., Chalar, C., Dauphin, Y., Massard, P., Pradel, P., and Marin, M. (2008) Monohydrocalcite in calcareous corpuscles of Mesocestoides corti. Exp. Parasitol, 118, 54–58.

Shannon, R.D. (1976) Revised effective ionic radii and systematic studies of interatomic distances in halides and chalcogenides. Acta Crystallographica Section A, 32, 751–767.

Sklyarov, E. V., Solotchina, E.P., Vologina, E.G., Ignatova, N. V., Izokh, O.P., Kulagina, N. V., Sklyarova, O.A., Solotchin, P.A., Stolpovskaya, V.N., Ukhova, N.N., and others (2010) Detailed Holocene climate record from the carbonate section of saline Lake Tsagan-Tyrm (West Baikal area). Russian Geology and Geophysics, 51, 237–258.

Solotchina, E.P., Prokopenko, A.A., Kuzmin, M.I., Solotchin, P.A., and Zhdanova, A.N. (2009) Climate signals in sediment mineralogy of Lake Baikal and Lake Hovsgol during the LGM-Holocene transition and the 1-Ma carbonate record from the HDP-04 drill core. Quaternary International, 205, 38–52.

Stoffers, P., and Fischbeck, R. (1974) Monohydrocalcite in the sediments of Lake Kivu (East Africa). Sedimentology, 21, 163–170.

Swainson, I.P. (2008) The structure of monohydrocalcite and the phase composition of the beachrock deposits of Lake Butler and Lake Fellmongery, South Australia. American Mineralogist, 93, 1014–1018.

Tanaka, J., Kawano, J., Nagai, T., and Teng, H. (2019) Transformation process of amorphous magnesium carbonate in aqueous solution. Journal of Mineralogical and Petrological Sciences, 114.

Taylor, G.F. (1975) The occurrence of monohydrocalcite in two small lakes in the south-east of South Australia. American Mineralogist, 60, 690–697.

Tollefsen, E., Stockmann, G., Skelton, A., Mörth, C.-M., Dupraz, C., and Sturkell, E. (2018) Chemical controls on ikaite formation. Mineralogical Magazine, 82, 1119–1129.

Tomić, Z.P., Makreski, P., and Gajić, B. (2010) Identification and spectra – structure determination of soil minerals : Raman study supported by IR spectroscopy and X-ray powder diffraction. Journal of Raman Spectroscopy, 41, 582–586.

Vereshchagin, O.S., Frank-Kamenetskaya, O. V, Shumilova, K. V, and Khadeeva, N.Y. (2018) Carbonate sediments on decorative fountains in Peterhof , Russia. Environmental Earth Sciences, 77, 1–10.

Wang, Y.Y., Yao, Q.Z., Zhou, G.T., and Fu, S.Q. (2015) Transformation of amorphous calcium carbonate into Monohydrocalcite in aqueous solution: A biomimetic mineralization study. European Journal of Mineralogy, 27, 717–729.

Yagi, S., and Fukushi, K. (2012) Removal of phosphate from solution by adsorption and precipitation of calcium phosphate onto monohydrocalcite. Journal of Colloid and Interface Science, 384, 128–136.

Zhang, G., Delgado-López, J.M., Choquesillo-Lazarte, D., and García-Ruiz, J.M. (2015) Growth behavior of monohydrocalcite (CaCO 3 ·H 2 O) in silica-rich alkaline solution. Crystal Growth and Design, 15, 564–572.

Zhang, G., Verdugo-Escamilla, C., Choquesillo-Lazarte, D., and García-Ruiz, J.M. (2018) Thermal assisted self-organization of calcium carbonate. Nature Communications, 9, 1–7.

Zou, Z., Habraken, W.J.E.M., Matveeva, G., Jensen, A.C.S., Bertinetti, L., Hood, M.A., Sun, C.-Y., Gilbert, P.U.P.A., Polishchuk, I., Pokroy, B., and others (2019) A hydrated crystalline calcium carbonate phase: Calcium carbonate hemihydrate. Science, 363, 396–400.

FIGURE CAPTIONS

Figure 1. Representative room temperature XRD patterns: (a) MHC ageing experiments (No 17; Table 2), (b) MHC and dypingite ageing experiments (No 30, Table 2), (c) aragonite and calcite ageing experiments (No 7, Table 2), (d) MHC spherules synthesised at various (1, 3, 6, 9) Mg/Ca ratio (No 9, 15, 21, 27; Table 2).

Figure 2. Unit cell parameters of synthesised MHCs depending on Mg/Ca ratio in initial solution: (a) parameter *a*, (b) parameter *c*. Symbols: square - syntheses at a temperature of 23 °C, round - syntheses at a temperature of 3 °C.

Figure 3. Representative Raman spectra: (a) calcite (No 6, Table 2), (b) aragonite (No 11, Table 2), (c) MHC (No 9; Table 2), (d) dypingite (No 16; Table 2).

Figure 4. Water content in MHC: (a) FTIR spectra, (b) integral area of H_2O band (2800-3700 cm^{-1} band *vs* Mg/Ca in solution).

Figure 5. Elemental map of MHC spherulite in MgKα and CaKα (No 15; Table 2).

Figure 6. SEM images of MHC: (a) connected spheres (No 15; Table 2), (b) aragonite overgrowth (bright) on MHC sphere (No 21; Table 2), (c) aragonite (bright) and dypingite (dark) overgrowth on MHC sphere (No 32; Table 2), (d) surface of MHC sphere (No 31; Table 2).

Figure 7. Representative EDX spectra: (a) calcite (No 14; Table 2), (b) aragonite (No 25; Table 2), (c) dypingite (No 29; Table 2).

Figure 8. Phase diagram for MHC, calcite, aragonite and dypingite precipitation at 23°C as a function of Mg concentration in solution and (a) initial pH, (b) final pH. Note solid fill – fields from initial pH, dashed fill – extended fields from final pH.

Figure 9.MHC crystal strucutre: (a) Ca1 and Ca3 ‘rods’ in *bc* projection, (b) Ca1, Ca2 and Ca3 ‘rods’ in *ab* projection.

Figure 10. Comparison of unit cell parameters of synthetic and natural MHCs.

SUPPLEMENTARY

Table S1. Dypingite indexing.

This is the peer-reviewed, final accepted version for American Mineralogist, published by the Mineralogical Society of America.
The published version is subject to change. Cite as Authors (Year) Title. American Mineralogist, in press.
DOI: https://doi.org/10.2138/am-2021-7673. http://www.minsocam.org/

Table 1. Experimental conditions of carbonates synthesis

No	Sample name	Exposure time, day	Mg, mmol /l	Mg/Ca solution	pH start	pH finish
T =23 °C						
1	CAM-53	35	0	0.0	9.35	9.53
2	CAM-80	21			9.64	9.68
3	CAM-81	22			10.98	10.45
4	CAM-91	24			11.76	11.67
5	CAM-38	29	5	0.5	10.15	9.90
6	CAM-40	29			10.90	10.41
7	CAM-93	23			11.65	10.37
8	CAM-39	29	10	1.0	9.83	9.80
9	CAM-22	19			10.71	10.88
10	CAM-37	29			11.03	10.88
11	CAM-92	23			11.59	11.10
12	CAM-25	14	20	2.0	9.82	9.62
13	CAM-23	19			10.55	10.88
14	CAM-51	21			10.76	11.01
15	CAM-24	21	30	3.0	10.48	10.76
16	CAM-26	14	40	4.0	9.74	9.46
17	CAM-15	6			10.32	10.44
18	CAM-52	21			10.35	10.78
19	CAM-29	22	50	5.0	10.16	10.39
20	CAM-27	14	60	6.0	9.77	9.55
21	CAM-30	22			10.13	10.30
22	CAM-90	21			10.72	10.09
23	CAM-31	22	70	7.0	10.12	10.21
24	CAM-28	14	80	8.0	9.83	9.48
25	CAM-16	7			10.17	10.36
26	CAM-97	38			10.42	10.27
27	CAM-32	22	90	9.0	10.04	10.03
28	CAM-35	32	100	10.0	9.62	9.37
29	CAM-36	31			10.24	10.20
30	CAM-88	21			10.48	9.70
31	CAM-87	21	120	12.0	10.04	9.70
32	CAM-89	21			10.59	9.80
T =3 °C						
33	CAM-7l	26	10	1.0	9.30	8.79
34	CAM-6l	26			10.25	9.09
35	CAM-2l	27			10.70	10.59
36	CAM-3l	30	40	4.0	9.25	9.09
37	CAM-4l	30			9.75	9.35
38	CAM-1l	20			10.32	9.67

Note: Ca =10 mmol /l, (CO_3) = 20 mmol /l.

This is the peer-reviewed, final accepted version for American Mineralogist, published by the Mineralogical Society of America.
The published version is subject to change. Cite as Authors (Year) Title. American Mineralogist, in press.
DOI: https://doi.org/10.2138/am-2021-7673. http://www.minsocam.org/

Table 2. Precipitations phase composition (according to PXRD), coherent scattering domain (CSD) and unit cell parameters (u.c.p.) of MHC.

No*	Mg/Ca solution	Phase composition (PXRD data), %	MHC u.c.p., Å		
			CSD, nm	*a*	*c*
		T =23 °C			
1	0	Cal 100			
2		Cal 100			
3		Cal 100			
4		Cal 100			
5	0.5	Cal 81, Ar 19			
6		Cal 82, Ar 18			
7		Cal 81, Ar 19			
8	1	Cal 80, Ar 10			
9		MHC 93, Cal 6, Ar 3	61	10.562(2)	7.508(5)
10		Ar 66, Cal 34			
11		Ar 71, Cal 29			
12	2	Cal 64, Ar 36			
13		MHC 95, Ar 5			
14		MHC 91, Ar 9	39	10.564(1)	7.501(3)
15	3	MHC 90, Ar 10			
16	4	Ar 57, Cal 43			
17		MHC 100			
18		MHC 95, Ar 5	28	10.558(1)	7.504(4)
19	5	MHC 97, Ar 3	35	10.558(2)	7.504(5)
20	6	Ar 69, Cal 31			
21		MHC 91, Ar 9	35	10.560(2)	7.506(5)
22		Dyp > MHC > Ar			
23	7	MHC 90, Ar 10	29	10.555(1)	7.514(3)
24	8	Ar 80, Cal 20			
25		MHC 82, Ar 18			
26		MHC 100	62	10.556(1)	7.513(2)
27	9	MHC 98, Ar 2	40	10.554(1)	7.517(4)
28	10	Ar 94, Cal 6			
29		MHC 100	39	10.554(1)	7.513(3)
30		MHC >> Dyp			
31	12	MHC 100	32	10.555(1)	7.522(4)
32		Dyp > MHC > Ar			
		T =3 °C			
33	1	Cal 93, Ar 7			
34		Cal 93, Ar 7			
35		MHC 100	29	10.563(1)	7.516(3)
36	4	Ar 63, Cal 30, MHC 7			
37		Ar 45, Cal 33, MHC 22			
38		MHC 100	41	10.559(1)	7.509(3)

Note: Weighted profile. R-factor (R_{wp}) was between 3–10%; as no structural data on dypingite are available only semi-quantitative results are present. * - numbers are the same as in Table 1. MHC – monohydrocalcite, Ar – aragonite, Cal – calcite, Dyp – dypingite.

Fig. 1

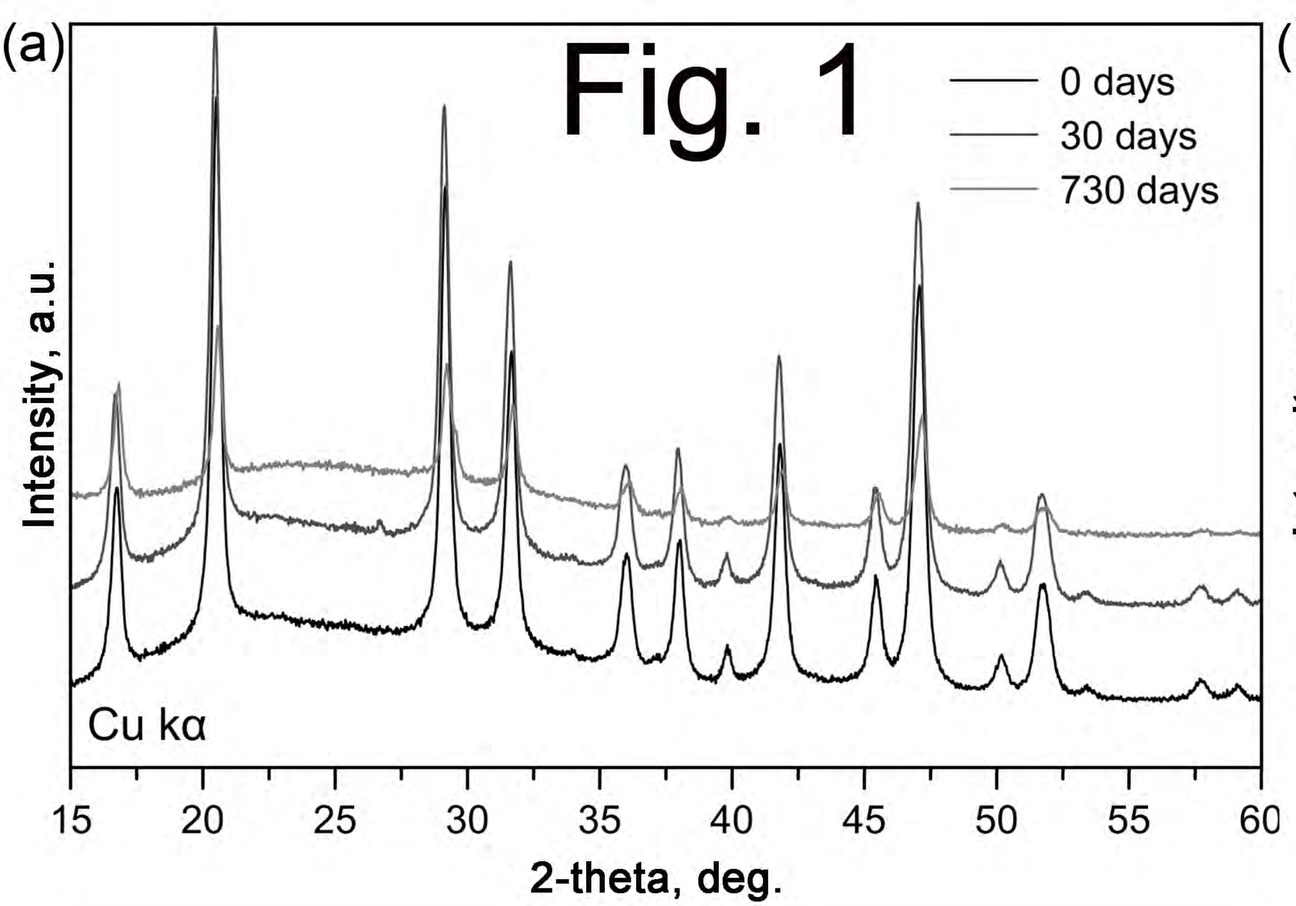
(a)
0 days
30 days
730 days
Intensity, a.u.
Cu kα
15 20 25 30 35 40 45 50 55 60
2-theta, deg.

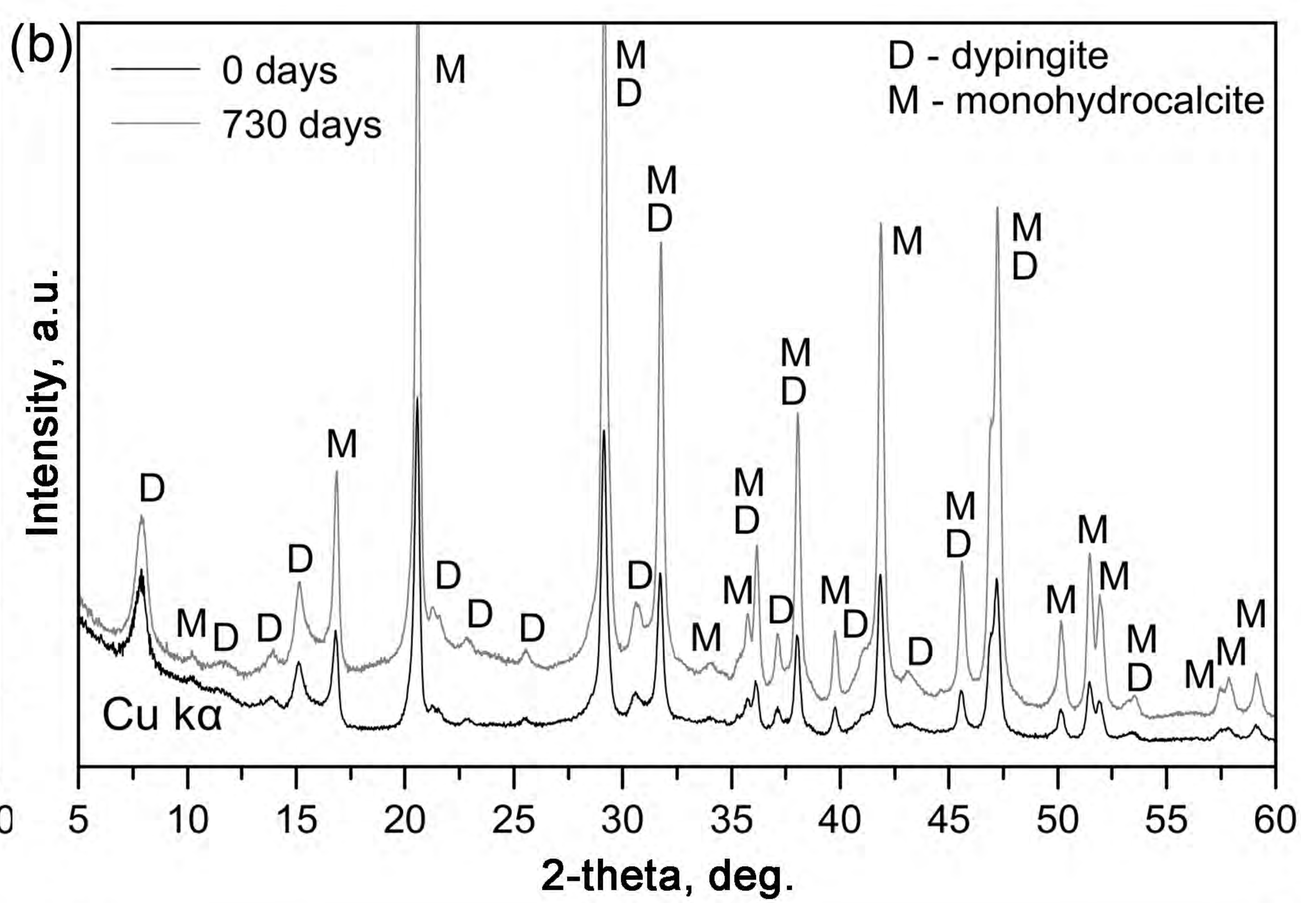
(b)
0 days
730 days
D - dypingite
M - monohydrocalcite
Intensity, a.u.
Cu kα
5 10 15 20 25 30 35 40 45 50 55 60
2-theta, deg.

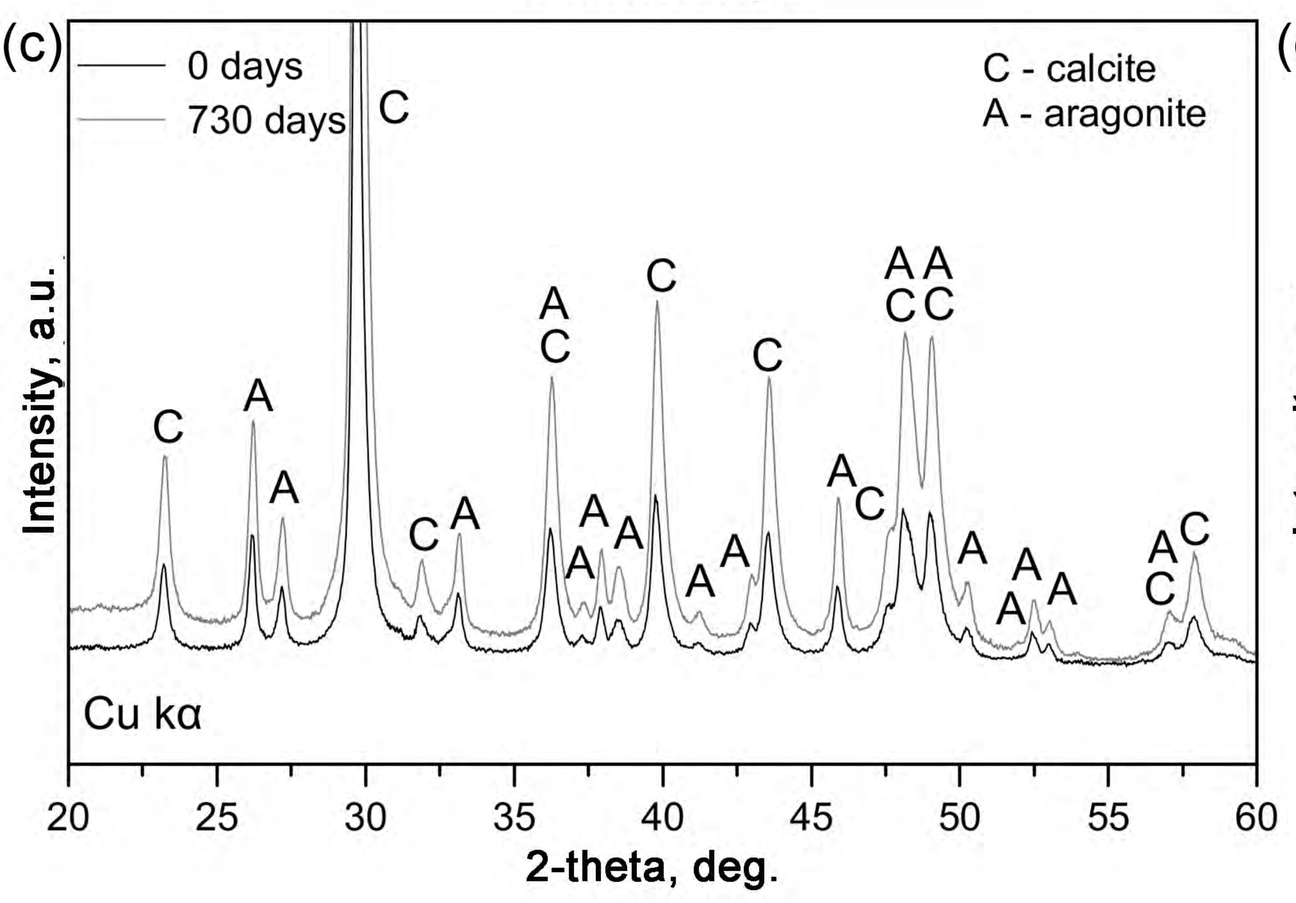
(c)
0 days
730 days
C - calcite
A - aragonite
Intensity, a.u.
Cu kα
20 25 30 35 40 45 50 55 60
2-theta, deg.

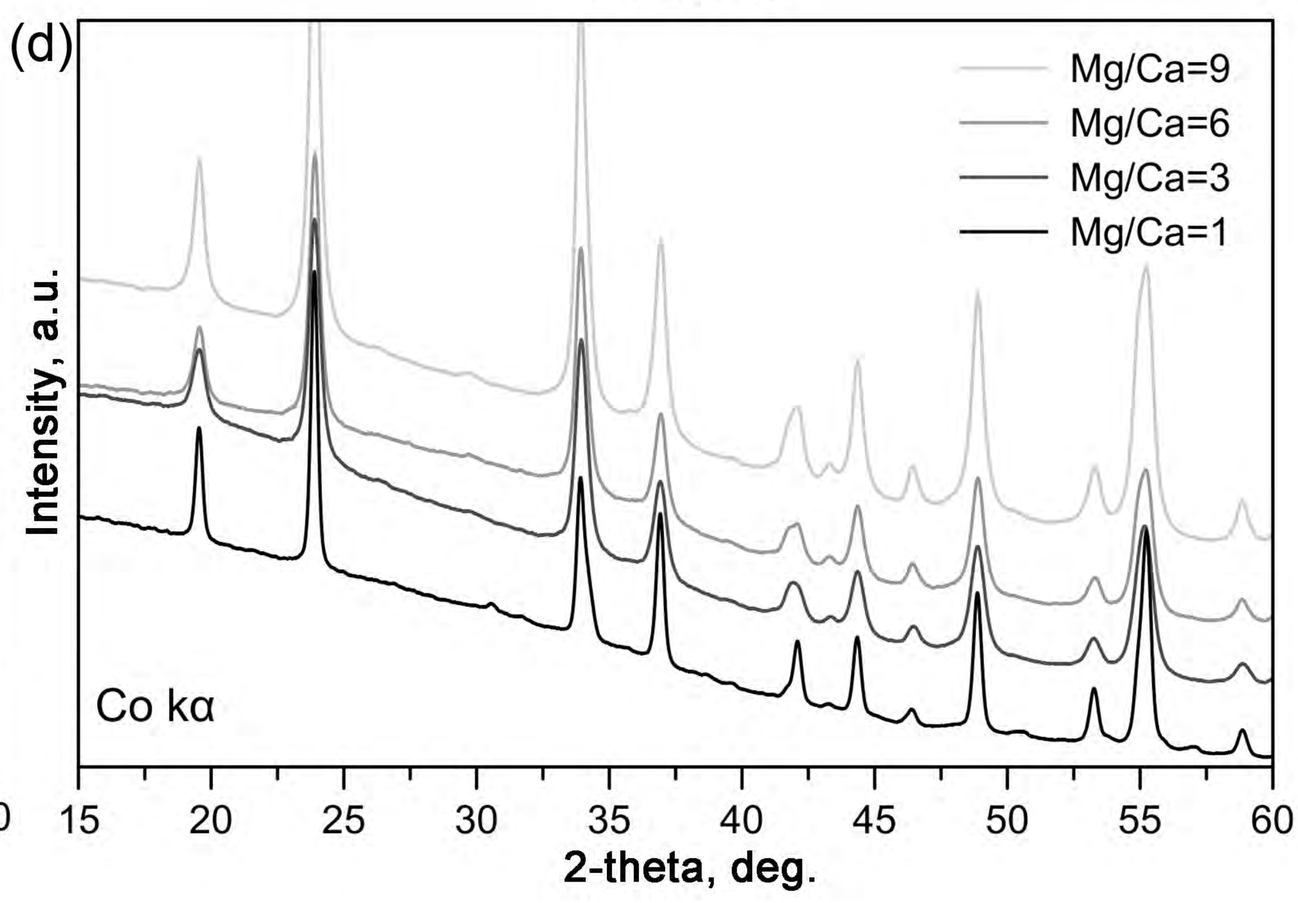
(d)
Mg/Ca=9
Mg/Ca=6
Mg/Ca=3
Mg/Ca=1
Intensity, a.u.
Co kα
15 20 25 30 35 40 45 50 55 60
2-theta, deg.

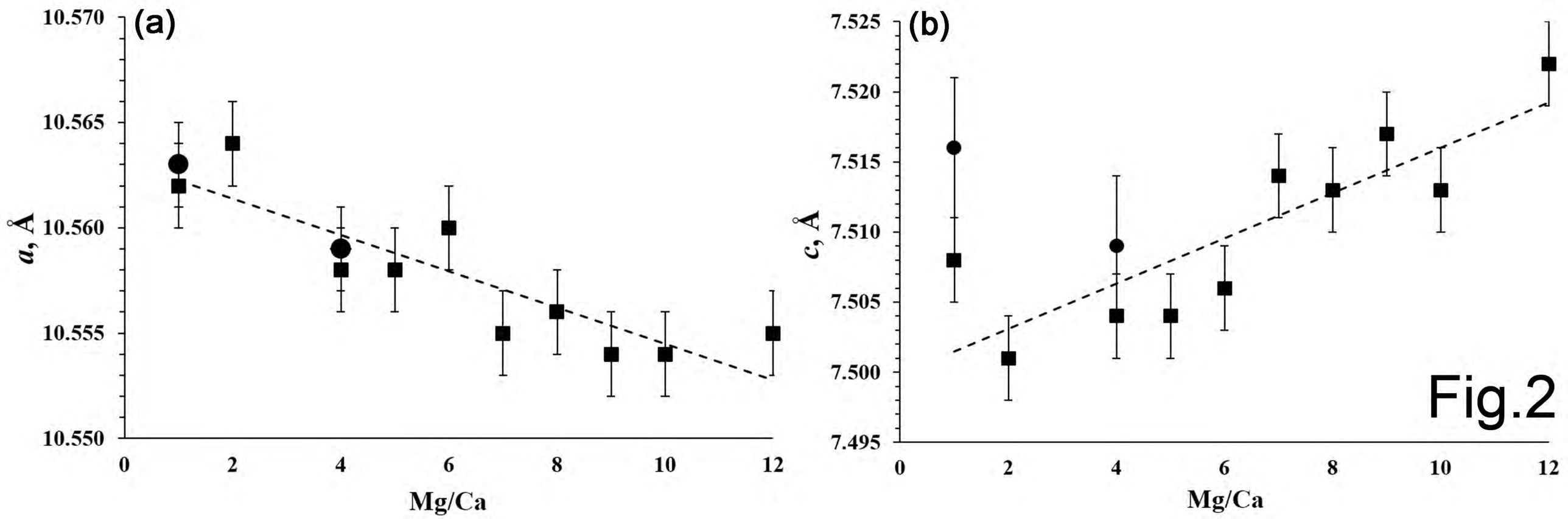
(a)
10.570
10.565
10.560
10.555
10.550
a, Å
0
2
4
6
8
10
12
Mg/Ca
(b)
7.525
7.520
7.515
7.510
7.505
7.500
7.495
c, Å
0
2
4
6
8
10
12
Mg/Ca

Fig.2

Fig. 3

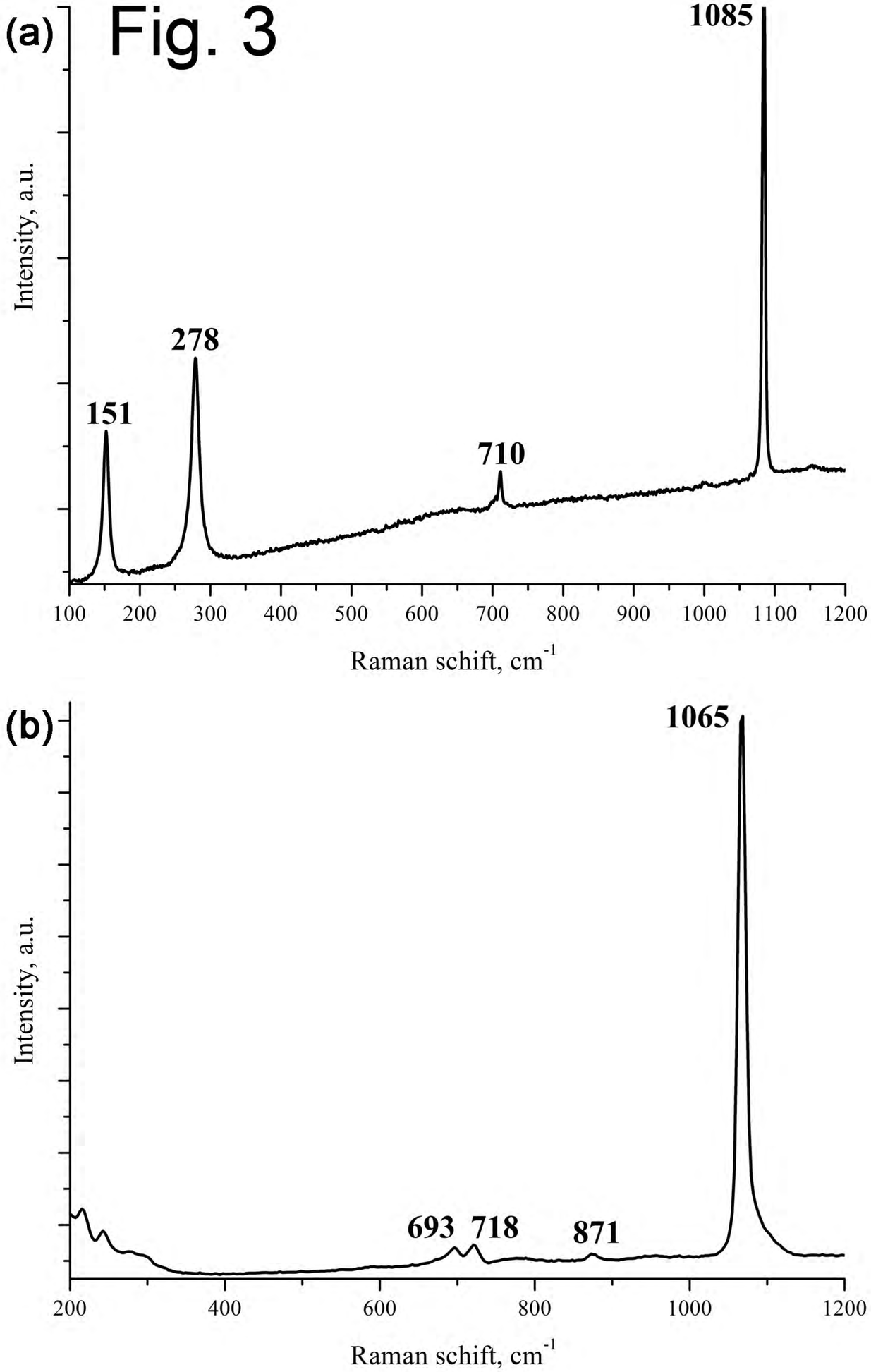
(a)
1085
278
151
710
Intensity, a.u.
100 200 300 400 500 600 700 800 900 1000 1100 1200
Raman schift, cm-1

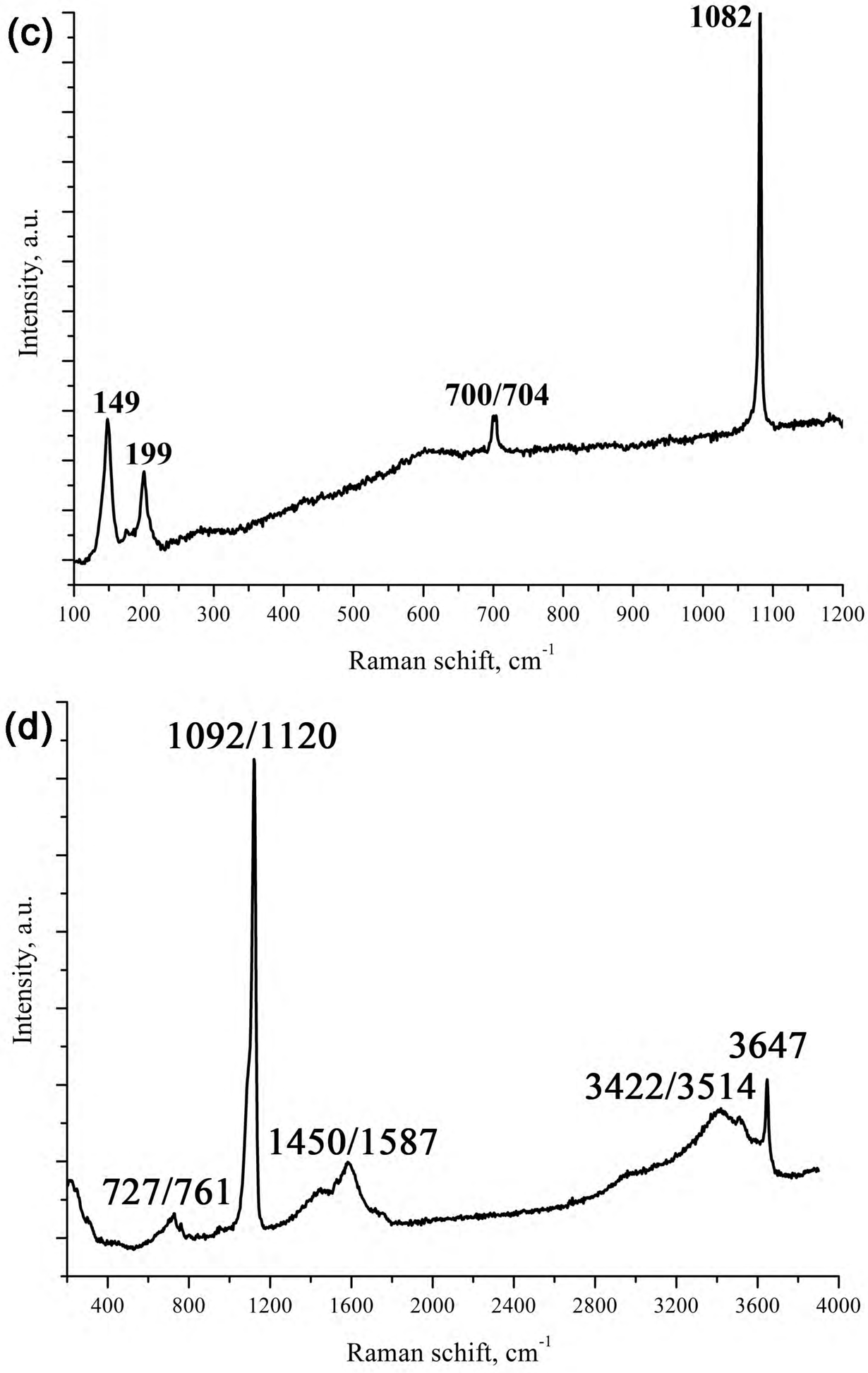
(c)
1082
149
199
700/704
Intensity, a.u.
100 200 300 400 500 600 700 800 900 1000 1100 1200
Raman schift, cm-1

(b)
1065
693
718
871
Intensity, a.u.
200 400 600 800 1000 1200
Raman schift, cm-1

(d)
1092/1120
3647
3422/3514
1450/1587
727/761
Intensity, a.u.
400 800 1200 1600 2000 2400 2800 3200 3600 4000
Raman schift, cm-1

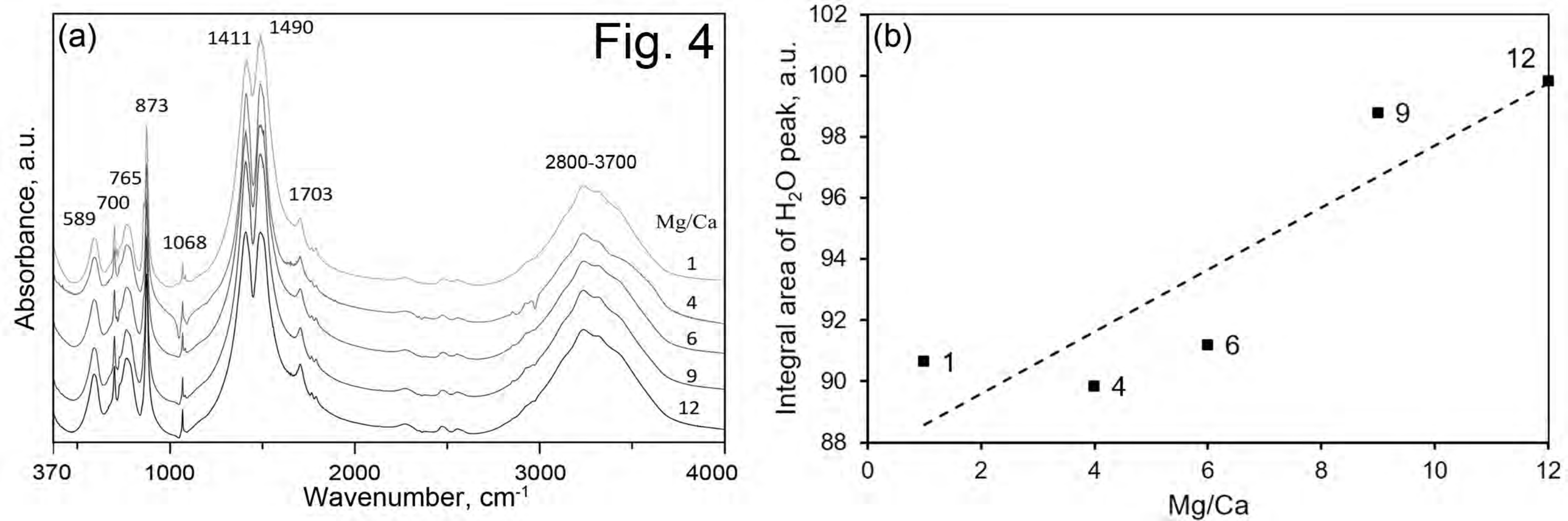
(a)
Fig. 4
1411
1490
873
765
700
589
1068
1703
2800-3700
Mg/Ca
1
4
6
9
12
Absorbance, a.u.
370
1000
2000
3000
4000
Wavenumber, cm-1
(b)
Integral area of H2O peak, a.u.
102
100
98
96
94
92
90
88
0
2
4
6
8
10
12
Mg/Ca

Fig. 5

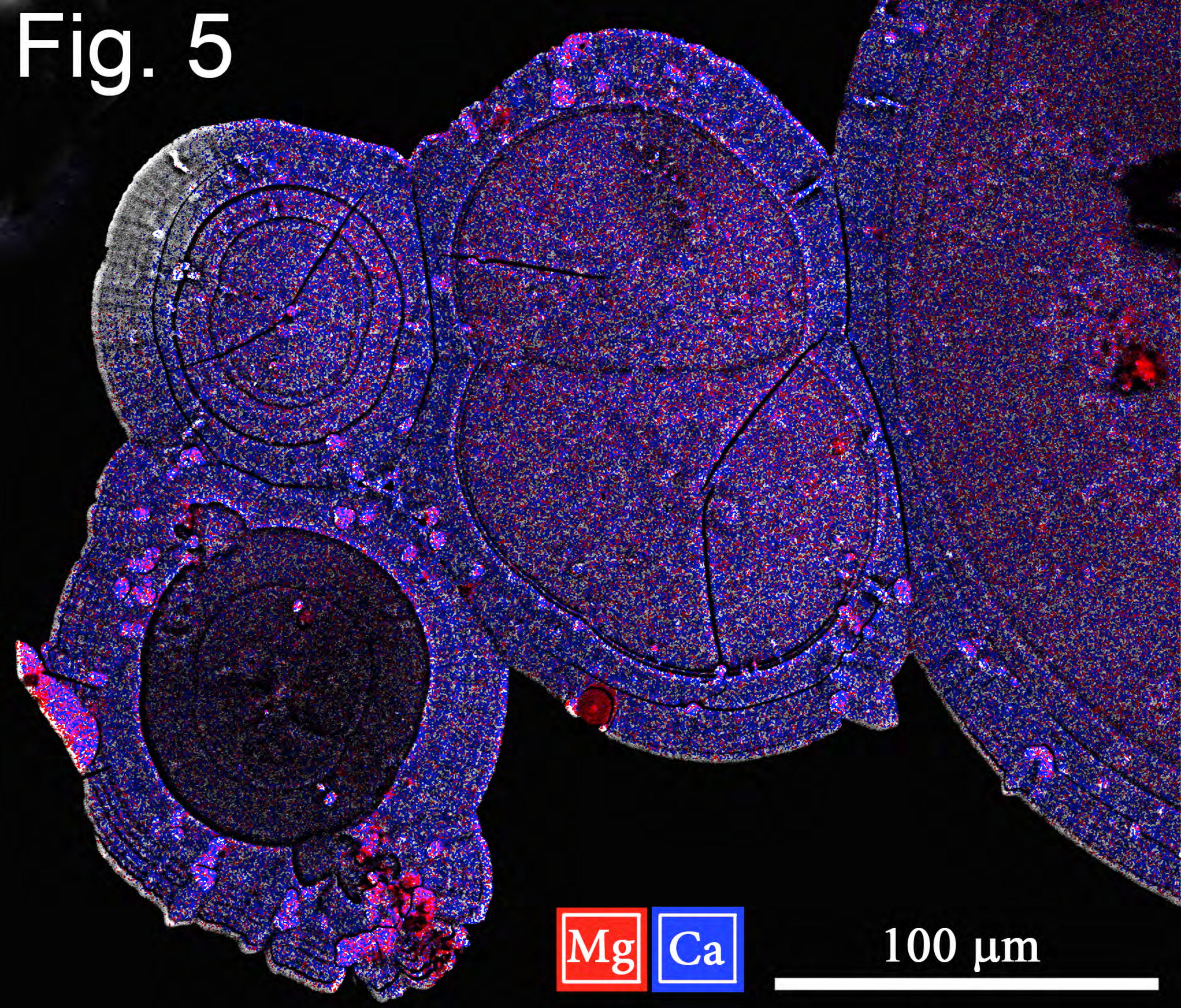

Fig. 6

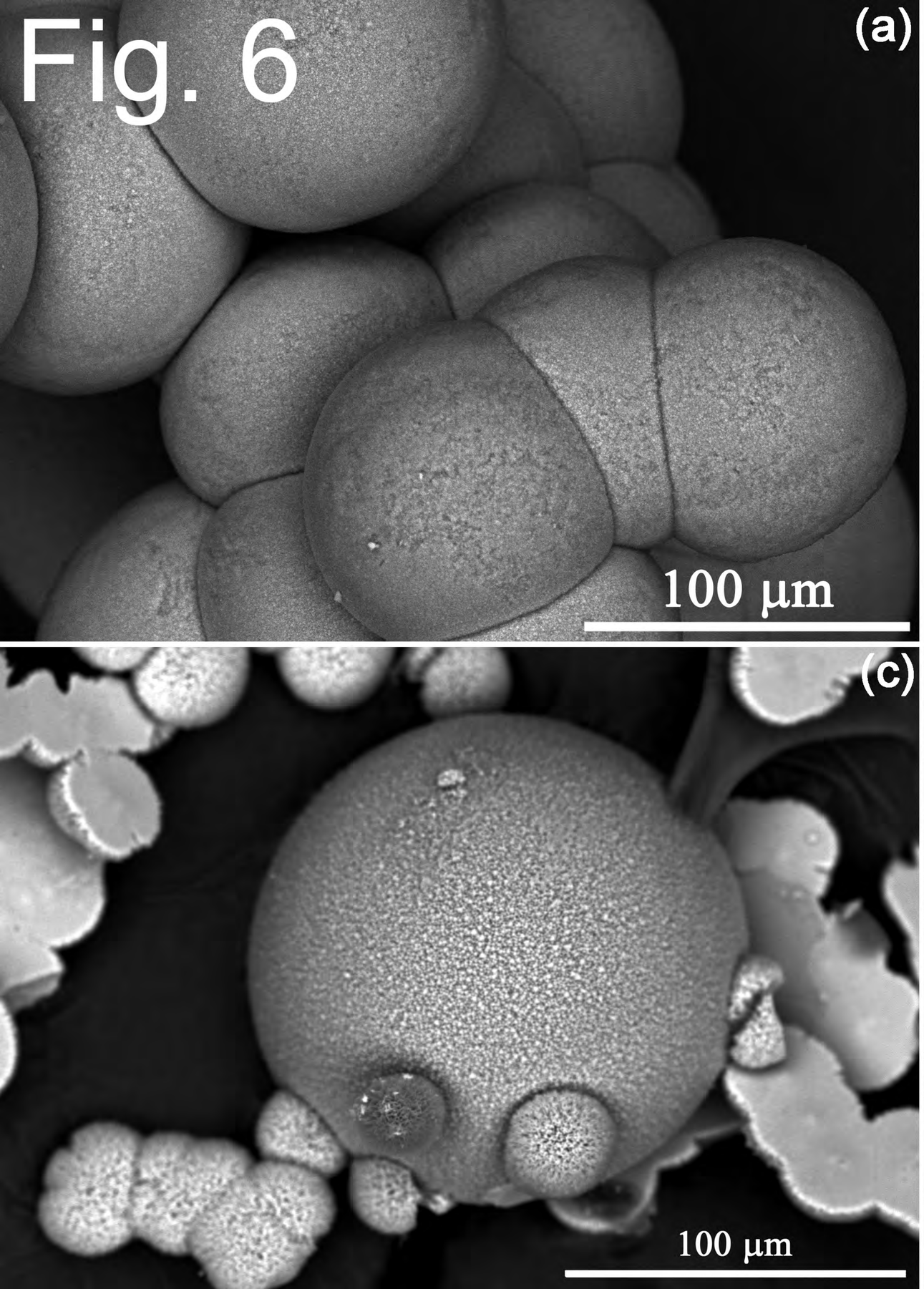

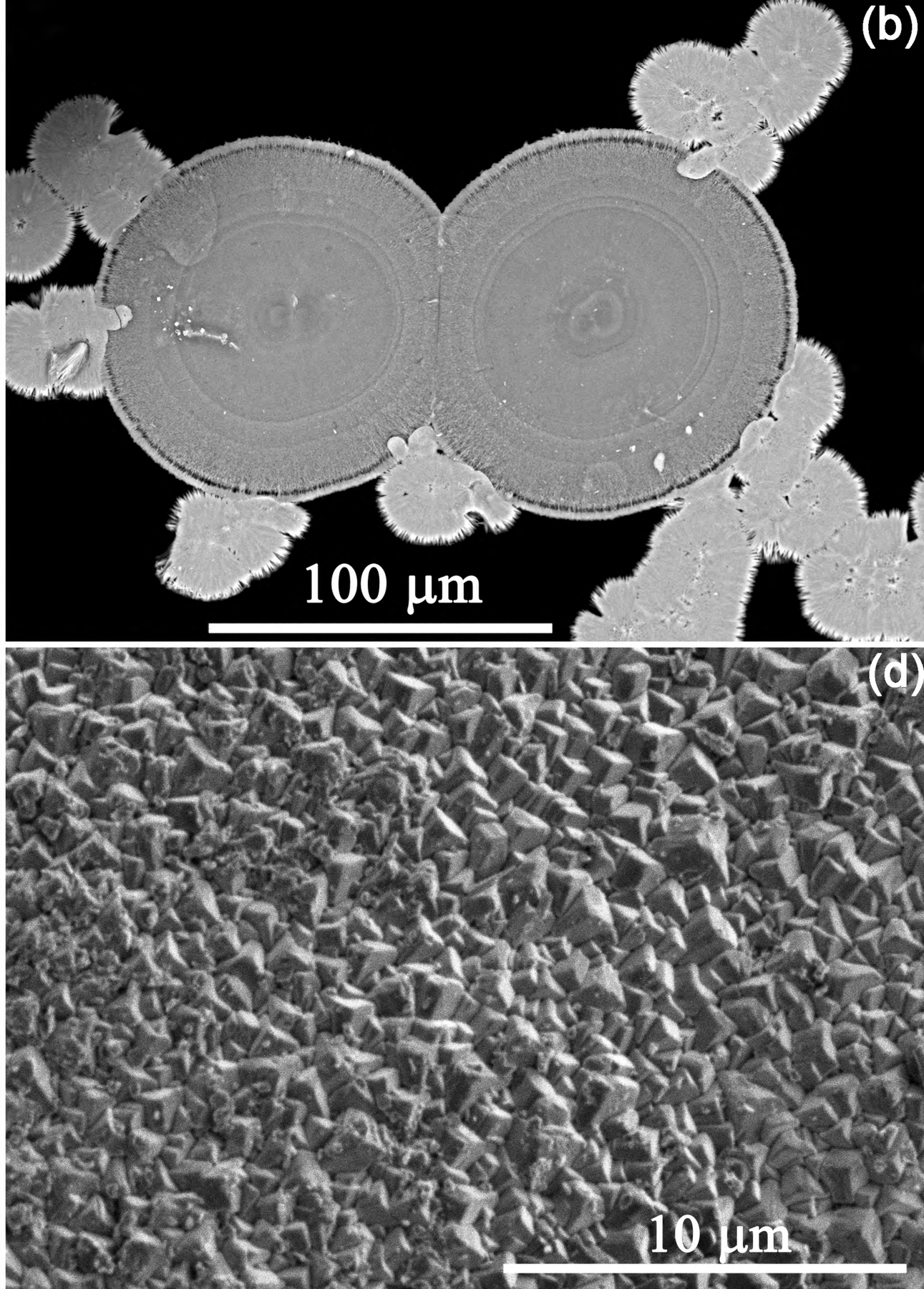

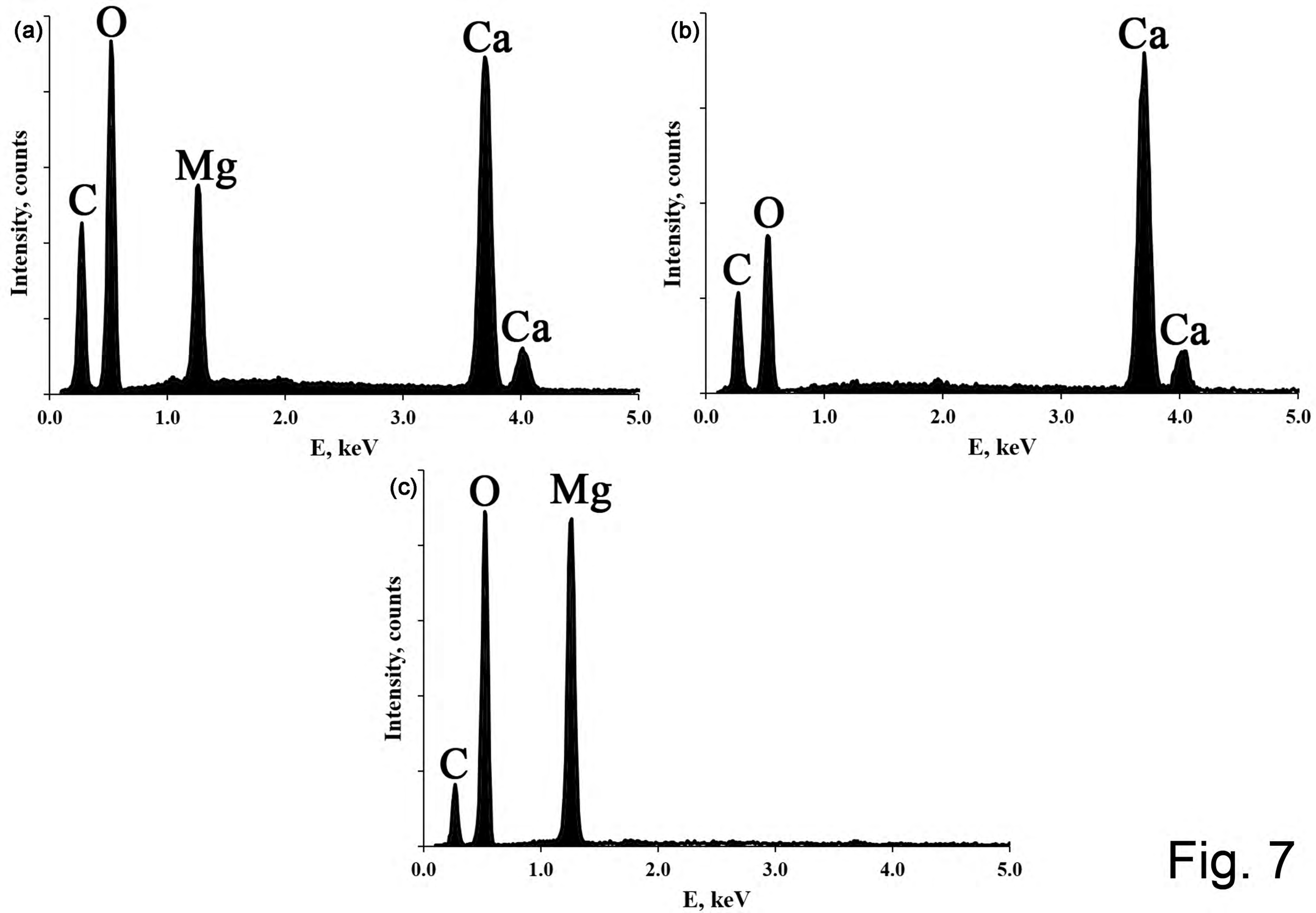
(a)
O
Ca
Mg
C
Ca
Intensity, counts
0.0
1.0
2.0
3.0
4.0
5.0
E, keV
(b)
Ca
O
C
Ca
Intensity, counts
0.0
1.0
2.0
3.0
4.0
5.0
E, keV
(c)
O
Mg
C
Intensity, counts
0.0
1.0
2.0
3.0
4.0
5.0
E, keV

Fig. 7

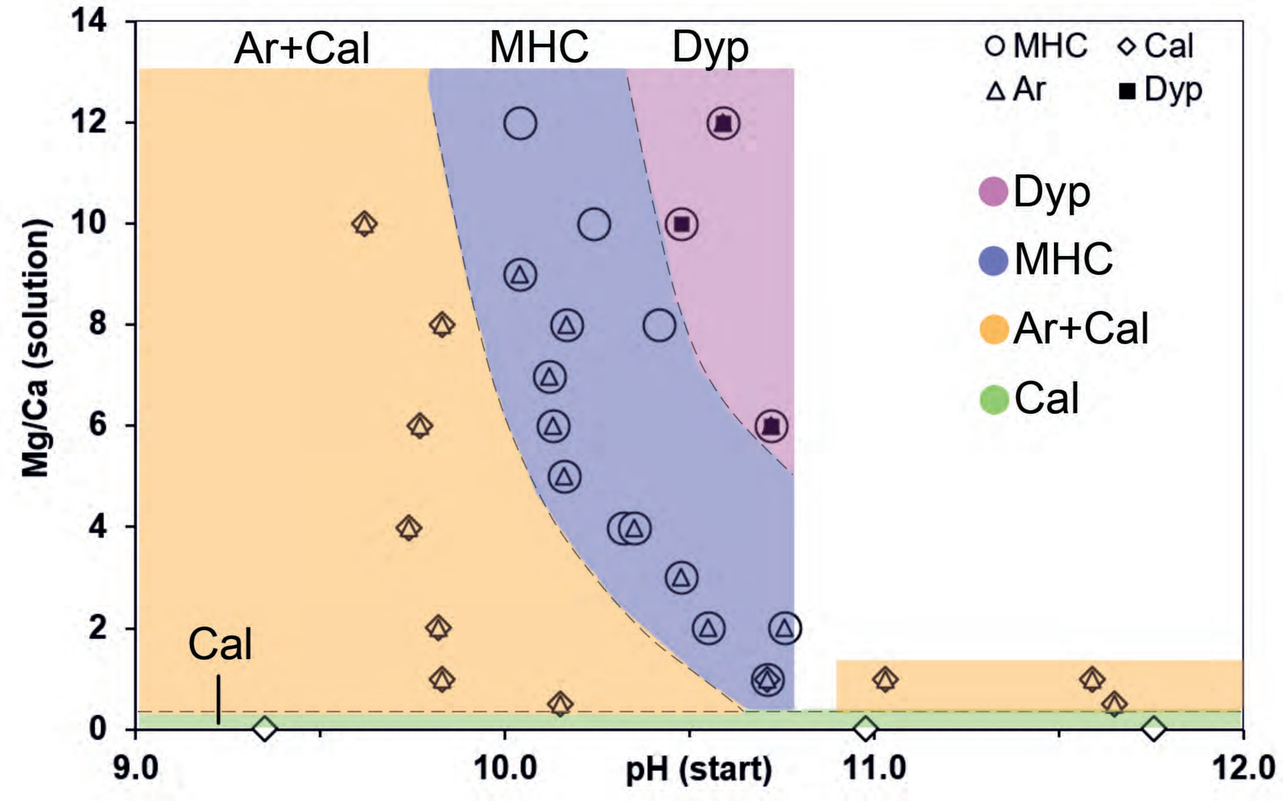
Ar+Cal
MHC
Dyp
MHC
Cal
Ar
Dyp
Dyp
MHC
Ar+Cal
Cal
Cal
Mg/Ca (solution)
pH (start)
0
2
4
6
8
10
12
14
9.0
10.0
11.0
12.0

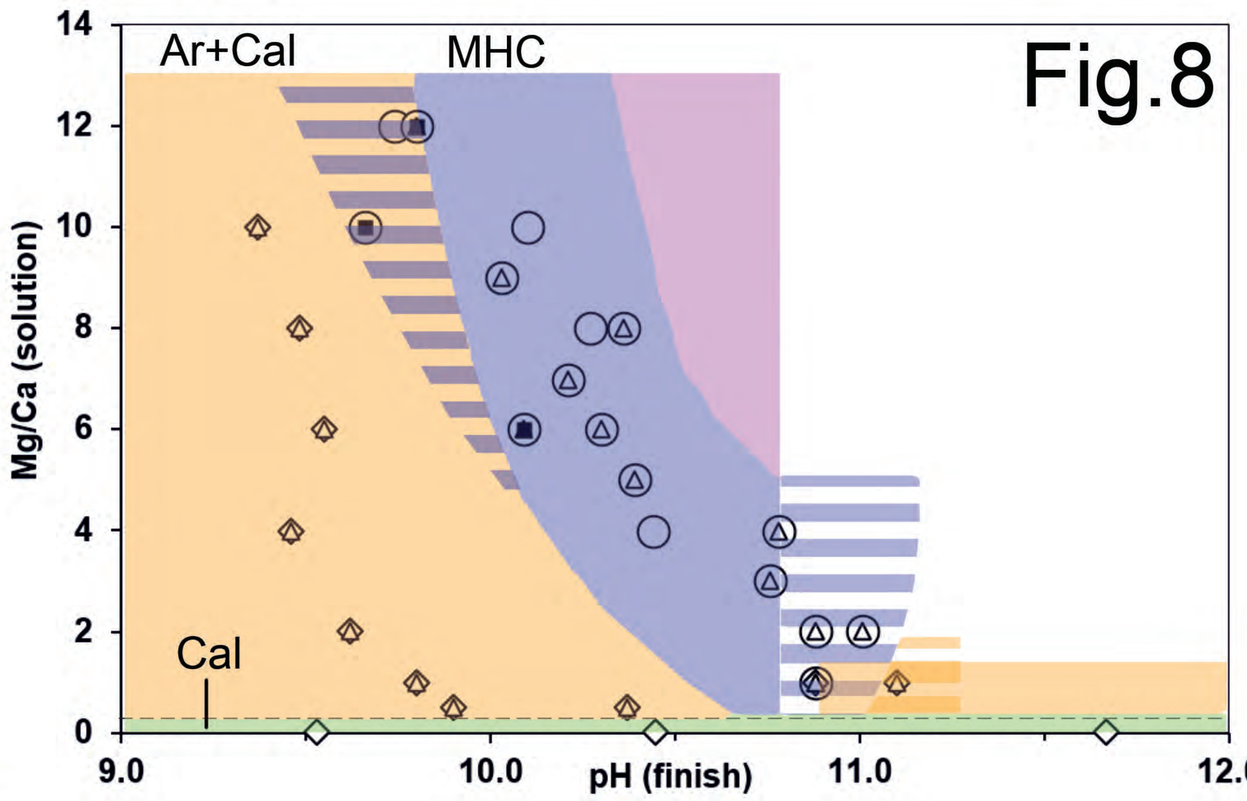
Ar+Cal
MHC
Cal
Mg/Ca (solution)
pH (finish)
0
2
4
6
8
10
12
14
9.0
10.0
11.0
12.0

Fig.8

Fig. 9

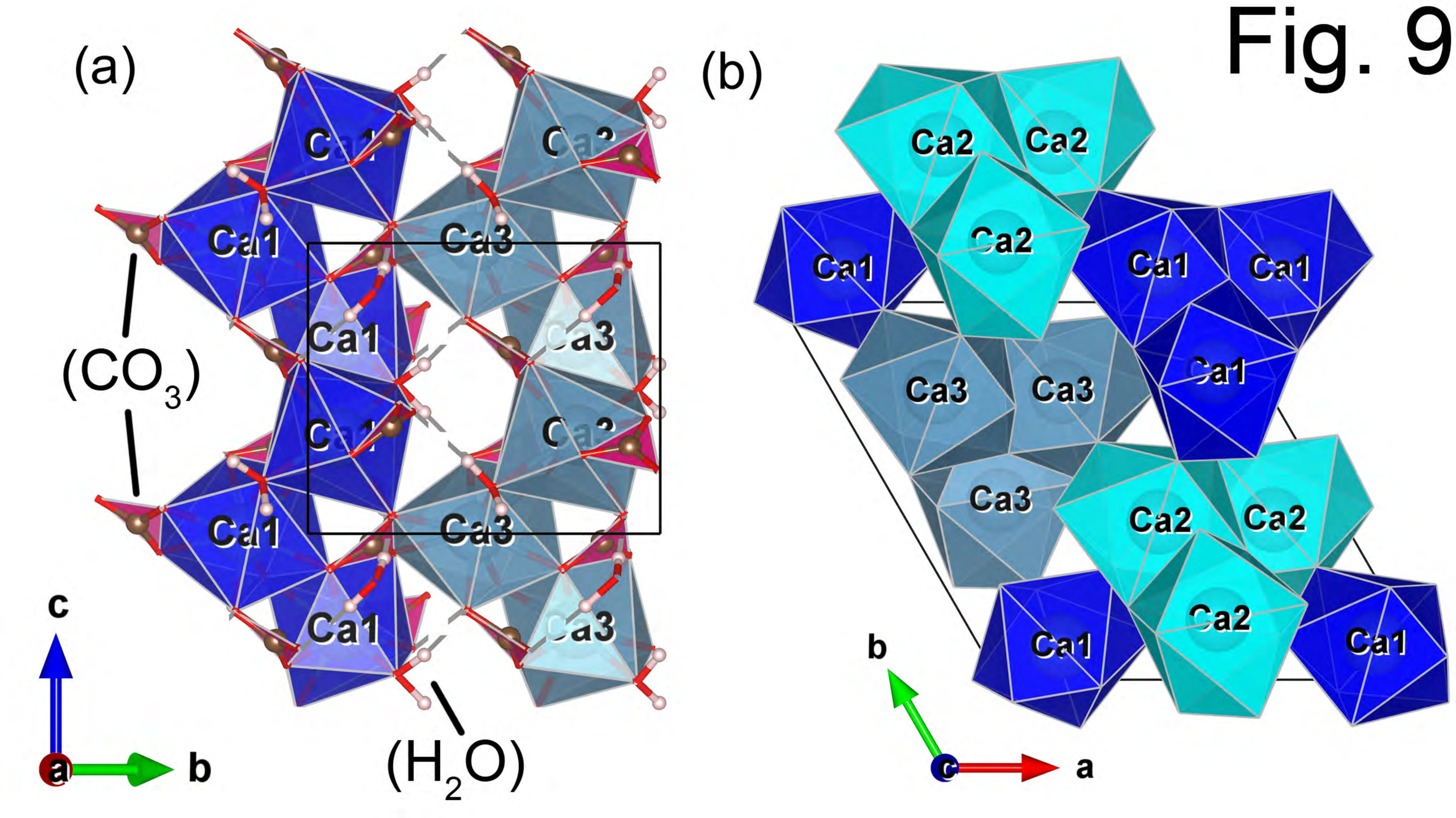

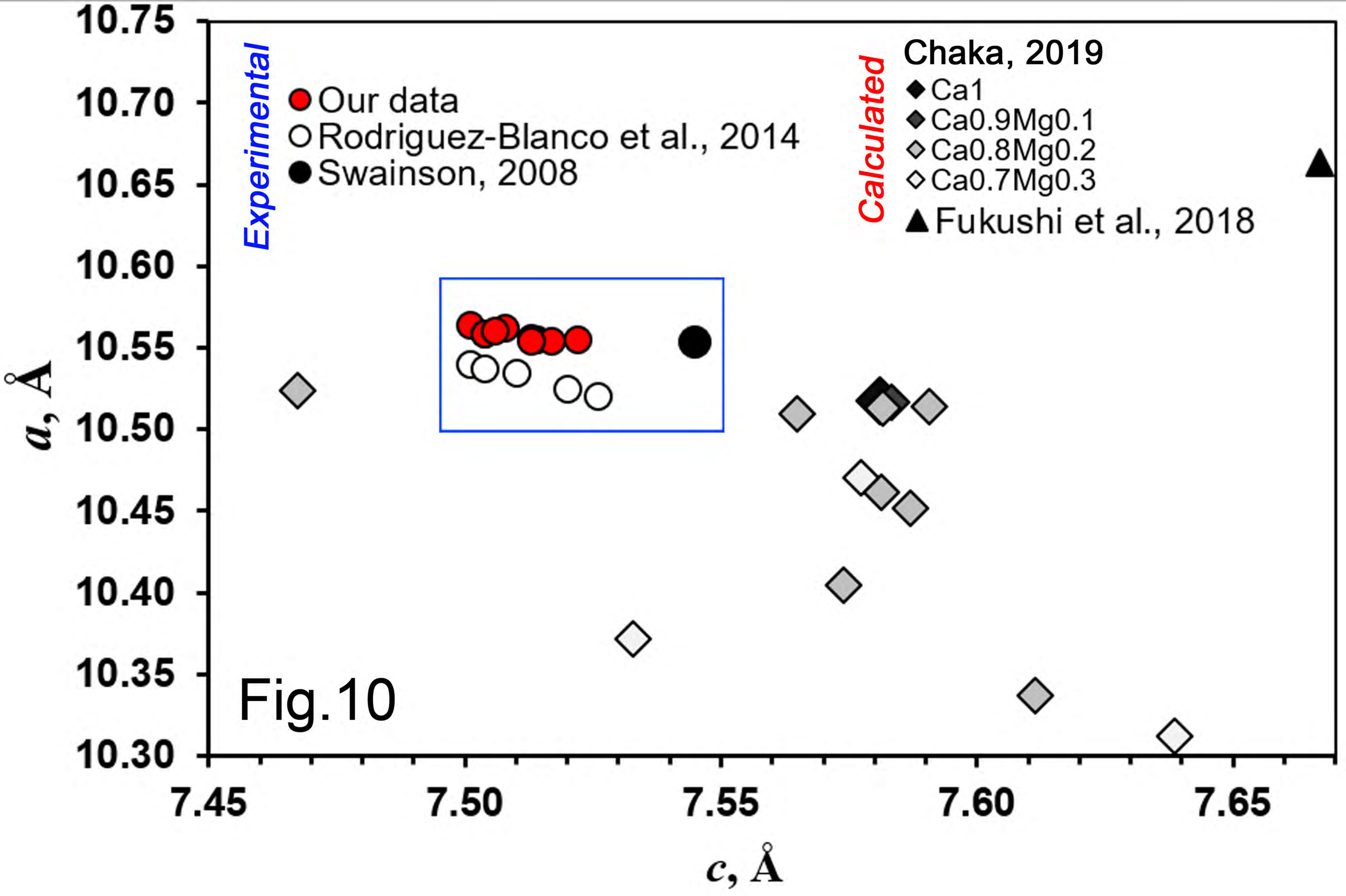
Experimental
Our data
Rodriguez-Blanco et al., 2014
Swainson, 2008
Calculated
Chaka, 2019
Ca1
Ca0.9Mg0.1
Ca0.8Mg0.2
Ca0.7Mg0.3
Fukushi et al., 2018
10.75
10.70
10.65
10.60
10.55
10.50
10.45
10.40
10.35
10.30
a, Å
7.45
7.50
7.55
7.60
7.65
c, Å

Fig.10